



**Materials in conducting suspension (semi-solid) electrodes  
for water and energy technologies**

Journal:	<i>Chemical Society Reviews</i>
Manuscript ID	CS-SYN-04-2015-000279.R2
Article Type:	Review Article
Date Submitted by the Author:	27-Aug-2015
Complete List of Authors:	Hatzell, Kelsey; 3141 Chestnut St, Material Science Boota, Muhammad; 3141 Chestnut St, Material Science and Engineering; Drexel University, Materials Science and Engineering Gogotsi, Yury; Drexel University, Material Science and Engineering



## Materials for suspension (semi-solid) electrodes for energy and water technologies

Kelsey B. Hatzell,<sup>a</sup> Muhammad Boota,<sup>a</sup> and Yury Gogotsi<sup>a</sup>

Received 00th January 20xx,  
Accepted 00th January 20xx

DOI: 10.1039/x0xx00000x

www.rsc.org/

Suspension or semi-solid electrodes have recently gained increased attention for large-scale applications such as grid energy storage, capacitive water deionization, and wastewater treatment. A suspension electrode is a multiphase material system comprised of an active (charge storing) material suspended in ionic solution (electrolyte). Gravimetrically, the electrolyte is the majority component and aids in physical transport of the active material. This principle enables, for the first time, scalability of electrochemical energy storage devices (supercapacitors and batteries) previously limited to small and medium scale applications. This critical review describes the ongoing material challenges encompassing suspension-based systems. The research described here combines classical aspects of electrochemistry, colloidal science, material science, fluid mechanics, and rheology to describe ion and charge percolation, adsorption of ions, and redox charge storage processes in suspension electrodes. This review summarizes the growing inventory of material systems, methods and practices used to characterize suspension electrodes, and describes universal material system properties (rheological, electrical, and electrochemical) that are pivotal in the design of high performing systems. A discussion of the primary challenges and future research directions is included.

### 1. Introduction

The demands for energy and fresh water are growing due to increasing consumption, growing population, and depleted supplies<sup>1, 2</sup>. Moreover, the interconnectedness ('nexus') between our water and energy critical infrastructures is drawing increasing attention because national and economic security is dependent on having sufficient supplies of both resources<sup>1</sup>. In industrialized countries, energy consumption is at an all-time high, and is projected to increase. It is anticipated that the US will require 4 to 5 terra kilowatt-hours of electricity annually by 2050.<sup>3</sup> Increased renewable energy generation and storage systems will be needed to accommodate this demand. Typically, critical infrastructures are large, centralized and require significant capital investments. For developing economies and rural environments these constraints often hinder widespread implementation. New versatile, sustainable, and affordable water technologies (wastewater treatment, water disinfection, decontamination, and desalination)<sup>1, 2, 4</sup> and energy technologies (generation and storage)<sup>5-7</sup> are needed to address growing needs across the globe.

Cost and lifetime are the guiding parameters for any infrastructure application<sup>8, 9</sup>. Flow-assisted electrochemical systems (FAES) are one route toward scalable and versatile energy storage. An example of a FAES is the redox flow battery (RFB) commonly explored for grid energy storage<sup>10</sup>. RFBs utilize a flowable architecture for decoupling energy and power densities. The size of the tanks determines the amount energy stored, while the number of cells (stack size) is directly related to the power density<sup>10-12</sup>. FAESs have been primarily limited to grid energy storage systems. Nevertheless, recent research on conducting suspension electrodes has enabled FAESs to be expanded to new applications such as water deionization<sup>13-18</sup>, energy storage<sup>19-24</sup>, energy generation<sup>25</sup>, and water

treatment<sup>26-28</sup> (**Fig. 1a-c**). Flow-architectures enable scalable systems and demonstrate decreasing costs with size through minimizing the costs of inactive materials (current collectors, separators, etc.).

Conducting suspension electrodes have a long history and have been studied in an array of electrochemical technologies<sup>29, 30</sup> related to wastewater treatment<sup>31, 32</sup>, electrodeposition<sup>33</sup>, electrolysis<sup>34</sup>, electrowinning of metals<sup>35, 36</sup>, and as a means for organic chemical synthesis<sup>37</sup>. The utilization of conducting suspension (fluidized-bed) electrodes for charge storage was studied for the first time in 1985, when Kastening et al. demonstrated charge transport (and storage) in porous graphite and activated carbon-based suspensions in sulfuric acid and potassium hydroxide electrolytes<sup>38, 39</sup>. Despite these early findings, the use of suspension electrodes for energy storage did not receive attention until 2011 (**Fig. 1**).

Due to parallel developments in both materials discovery, and materials processing, suspension-based electrodes have recently re-emerged in energy storage technologies (**Fig. 1a**). Since the semi-solid flow battery (SSFB) was introduced as a way to utilize intercalation materials (faradic charge storage) for flowable large scale energy storage<sup>19</sup>, research has increased significantly in this area. The SSFB directly addresses the limitations of RFBs - energy density. RFBs are limited by the cost and solubility of metal redox species in aqueous/non-aqueous solutions (~2M concentrations). The SSFB addresses this concentration limitation, and has the ability to achieve 10-40 M concentrations<sup>19</sup>. This demonstration has led to significant growth in research related to suspension electrodes, and the number of academic publications has increased 4-fold since 01/2013 (Web of Science). Suspension (or semi-solid) electrodes are electronically conducting, in contrast to insulating RFB systems. In a suspension electrode, the active material (charge storing) is not soluble but suspended in an electrolyte, and electron transport occurs through the formation of percolation networks of agglomerated active materials (particles). The flowing of suspended material allows for continuous charge storage or ion removal (**Fig. 1c**).

<sup>a</sup>A.J. Drexel Nanomaterials Institute and Department of Material Science and Engineering, Drexel University, 3141 Chestnut Street, Philadelphia, Pennsylvania 19104, USA.

Significant progress can be made in suspension electrodes guided by a greater understanding of properties of materials and material systems that promote efficient charge storage and electron conduction (Fig. 1). For large scale applications, materials need to be low-cost, abundant, and non-toxic to compete with current technologies. This review details the current scientific progress toward functional suspension systems in an array of applications. Specifically, this work emphasizes the need for tailored materials (by application) and a holistic understanding of how the inactive and active materials interact in order to guide the design of suspension electrodes. Section 2 provides an overview of the various applications that utilize suspension electrodes, and the specific role (mechanism) the active material serves. In Section 3, we review the materials literature related to electrochemical energy storage systems specifically focusing on the semi-solid flow battery and the electrochemical flow capacitor. In Section 4, we describe materials for water technologies and describe the recent progress made in applications such as capacitive deionization (Fig. 1c), capacitive mixing, and microbial fuel cells (Fig. 1b) based on suspension electrodes. Section 5 summarizes multi-physics modelling and theoretical approaches toward understanding how a suspension electrodes can optimally be integrated into a flow architecture. In Section 6, we provide an overview of the rheological, electrical, and electrochemical properties of suspension electrodes and the primary methods for characterizing each of these properties. Across each section, there is an emphasis on describing how the active and inactive materials can coexist in a mutualistic and harmonious fashion.

## 2. Applications for conducting suspension electrodes

RFBs and stationary battery systems (lithium-ion, sodium-sulfur, and lead-acid) have been examined as electrochemical energy storage solutions for the grid<sup>5</sup>. In RFBs, the active material (species) is dissolved in a liquid electrolyte. A host of different redox pairs<sup>10, 40</sup> have been reported, and the all-vanadium sulfate RFB (VRFB)<sup>11, 12, 41</sup> is one of the leading technologies to be commercialized to date<sup>42</sup>. This is in part because the  $V^{2+}/V^{3+}$  and  $V^{4+}/V^{5+}$  (and  $VO^{2+}/VO^{+2}$ ) redox couples in sulfate solutions demonstrate favorable reversibility and are well understood kinetically<sup>43</sup>. For large scale energy storage, the materials cost need to be low ( $< \$2 \text{ kg}^{-1}$ ), and the commodity cost of Vanadium is  $\sim \$23 \text{ kg}^{-1}$ <sup>42</sup>. Moreover VRFBs are limited by solubility  $< 2\text{M}$  (energy density  $\sim 25 \text{ Wh kg}^{-1} / \sim 40 \text{ Wh L}^{-1}$ ) and operating temperatures between  $10\text{-}40^\circ\text{C}$ <sup>44</sup>. All these aspects combined motivate exploring alternative technologies.

Battery technologies based on high capacity intercalation materials such as  $\text{LiFePO}_4$  with a theoretical capacity of  $170 \text{ mAh g}^{-1}$ <sup>45, 46</sup> and energy density of  $550 \text{ Wh kg}^{-1}$ <sup>47</sup>, are capable of addressing capacity needs. Nevertheless, scale up of lithium-ion battery technologies becomes costly because of the high cost of inactive materials necessary when connecting 1000s of batteries together in a pack. To overcome this challenge, Duduta et al. demonstrated that typical battery cathode materials could be used in a flowable suspension media in a technology called the semi-solid flow battery (SSFB). Instead of using soluble redox-species, solid active material can be suspended in an electrolyte and flowed through the characteristic RFB flow architecture depicted in Fig. 1a. The use of suspension electrodes opens a wider portfolio of possible (energy-dense or power-dense) material chemistries that can be examined for grid energy storage applications. Examples of this broadening material portfolio include crystalline materials showing intercalation

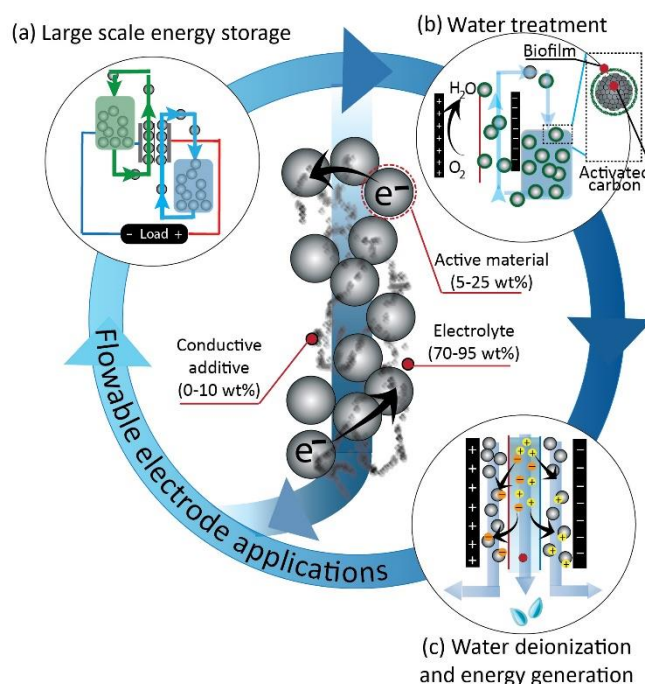


**Fig. 1.** Compositional make-up and applications for flowable suspension electrodes. Suspension electrodes are composed of a charge storing (active) material, a conductive additive, and an ion containing solution (electrolyte). The compositional make-up affects the obtainable capacity and flowability. Flowable electrodes based on faradic (battery) and electrostatic (supercapacitor) charge storage mechanisms have been examined for large-scale energy storage applications (a). Capacitive suspension electrodes have been demonstrated for water treatment (b) and water deionization/energy generation (c).

properties  $\text{LiFePO}_4$  (LFP)/ $\text{LiCoO}_2$  (LCO), etc.<sup>19, 24</sup>, precipitation-dissolution chemistries (Li-sulfur<sup>22</sup>, Mn-sulfur<sup>48</sup>), electrodeposition redox-chemistries<sup>49, 50</sup>, carbon based electrochemical capacitors<sup>51, 52</sup> and pseudocapacitors<sup>20, 21</sup>, and hybrid electroplating-polymer systems ( $\text{Zn/PANi}$ <sup>53, 54</sup>,  $\text{MnO}_2/\text{PPy}$ <sup>55</sup>).

The active materials role in electrochemical energy storage applications is to store charge. The two primary modes for achieving this goal is through faradic (chemical)<sup>56</sup> processes or electrostatically through the adsorption of electrolyte ions onto the surface of the active electrode material<sup>51, 57</sup>. LIBs and SSFBs use the former mechanism and rely on the insertion of  $\text{Li}^+$  ions into the electrode material to initiate redox reactions. This process is diffusion controlled, and thus limits battery-type electrode to low-rate applications<sup>58</sup>. In contrast, supercapacitors (electric double-layer capacitors) store charge via fast and reversible adsorption of ions at the active material interface. Supercapacitors are limited in terms of energy density because charge storage only occurs at the available and accessible active material surface area<sup>51, 59</sup>. Nevertheless, they show notable performance in terms of power density. The Gogotsi group recently demonstrated that supercapacitors (electrochemical capacitors) could be scaled up for grid energy storage applications through the utilization of high specific surface area activated carbon suspended in an aqueous electrolyte in a technology called the electrochemical flow capacitor (EFC)<sup>21</sup>.

Since the early demonstrations of suspension electrodes for electrochemical energy storage in 2011, an array of different existing technologies have integrated suspension electrodes in order to improve scalability limitations. All-carbon based suspension electrodes have been introduced for flow-electrode capacitive

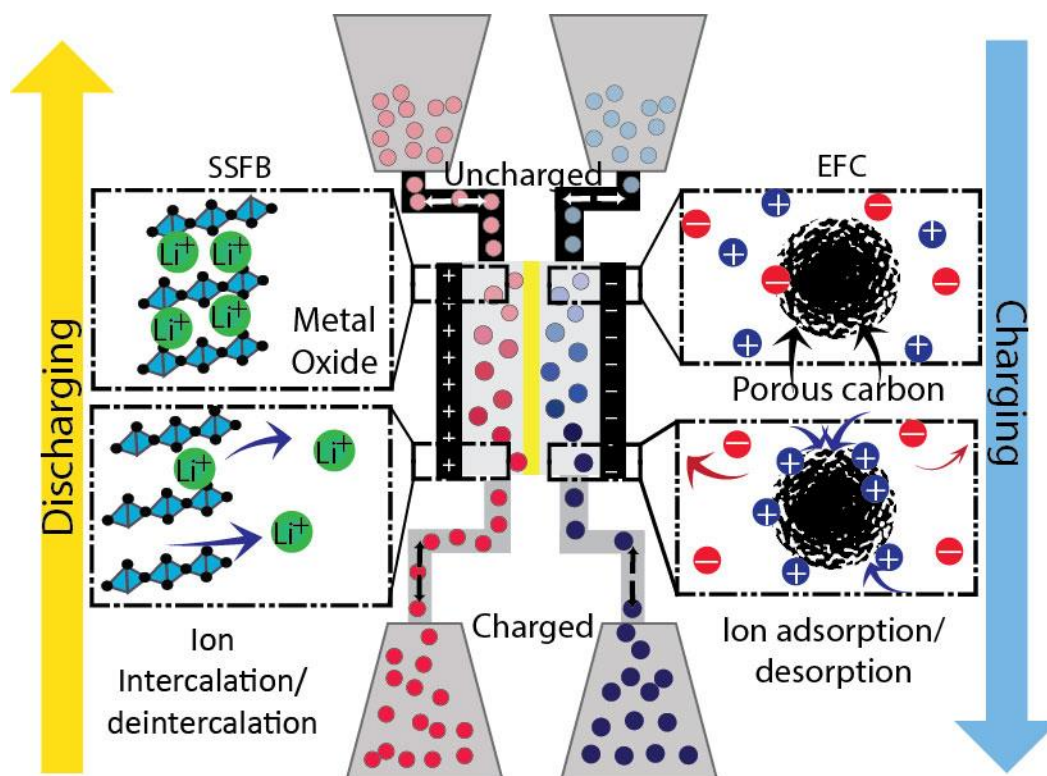


**Fig. 2.** A characteristic flow architecture utilized for large-scale energy storage based on suspension (semi-solid) electrodes. The semi-solid flow battery (SSFB) utilizes faradic charge storage mechanisms with ion intercalation and de-intercalation mechanisms during discharging and charging processes. The electrochemical flow capacitor (EFC) stores charge electrostatically in an electric double layer at the active material surface. The charging cell is composed of two current collectors and an ion-permeable (electron insulating) separator. Four tanks are utilized, two for storing uncharged suspensions, and two for charged suspensions.

deionization<sup>13, 16</sup> (ion-removal) and capacitive mixing<sup>18, 25</sup> (energy generation) systems. The primary benefit of using suspension (flow-electrodes) over stationary film electrodes, is for scalable and controllable ion removal in capacitive deionization (CDI) and constant power output in capacitive mixing (CapMix)<sup>60, 61</sup>. The primary role of the active materials in CDI is for ion removal, thus it has been shown to be advantageous to have materials that are conducting and exhibit high specific volumes among the micropores<sup>62</sup>. In CapMix, energy is generated (and harvested) through the expansion and contraction of the electric double layer formed at the surface of the active material. The extent of this expansion and contraction (and subsequent energy generation) is proportional to the surface charge density of the active material. Thus, it has been shown to be advantageous to have asymmetric anode and cathode materials that display capacitive behaviors and are characterized by different rise potentials<sup>60, 63</sup>. Finally, the most recent system utilizing suspension electrodes is in the field of water treatment. Microbial fuel cells (MFCs) are a technology currently being examined for simultaneous wastewater treatment and energy recovery (**Fig. 1b**). In a MFC, exoelectrogenic bacteria decompose organics in wastewater, and convert that chemical energy into electricity (energy generation)<sup>64, 65</sup>. This technology has been sought out as a way to decrease the energy consumed during wastewater treatment. Recently, this technology adopted carbon-based suspension electrodes in place of a static anode, in order to increase the system size. In this application, the material's role is as a biofilm carrier and host for efficient organic decomposition (and electron storage)<sup>26, 27</sup>.

For each application described above, there are different requirements for the active material. There is a need for designing conducting materials for charge storage, ion removal, tailored surface charge densities, and effective biofilm growth purposes. Undoubtedly, one material cannot serve all these needs. Moreover, as suspension electrodes are 'material systems' composed of active and inactive materials it is necessary to strike a synergistic balance between both active and inactive materials in the design of high performing suspension electrodes<sup>66</sup>.

### 3. Suspension electrode applications in electrochemical energy storage

There are two types of suspension-based flow systems currently being explored for grid energy storage: (1) the electrochemical flow capacitor (EFC) and (2) the semi-solid flow battery (SSFB)<sup>19</sup>. Both systems use a flow architecture similar to RFBs (**Fig. 2**). The primary difference between the SSFB (or EFC) and RFBs is that active material is suspended, rather than dissolved in a solution (**Fig. 1**). Typically, the active material content is between 5-25 wt% (**Fig. 1**). While it is ideal to have higher active loading, flowability is a fundamental limitation and has been shown to decrease drastically above 20 wt% and depend on the size, shape, composition of the active particles.<sup>67</sup> **Fig. 2** demonstrates the concept of flow-assisted electrochemical energy storage based on suspension electrodes. In the SSFB, the cathodic suspension enters the electroactive region fully intercalated and is exposed to an applied voltage as it flows through the working cell. As a result, the working cations become deintercalated and transported to the anode suspension which induces a flow of electrons (current).

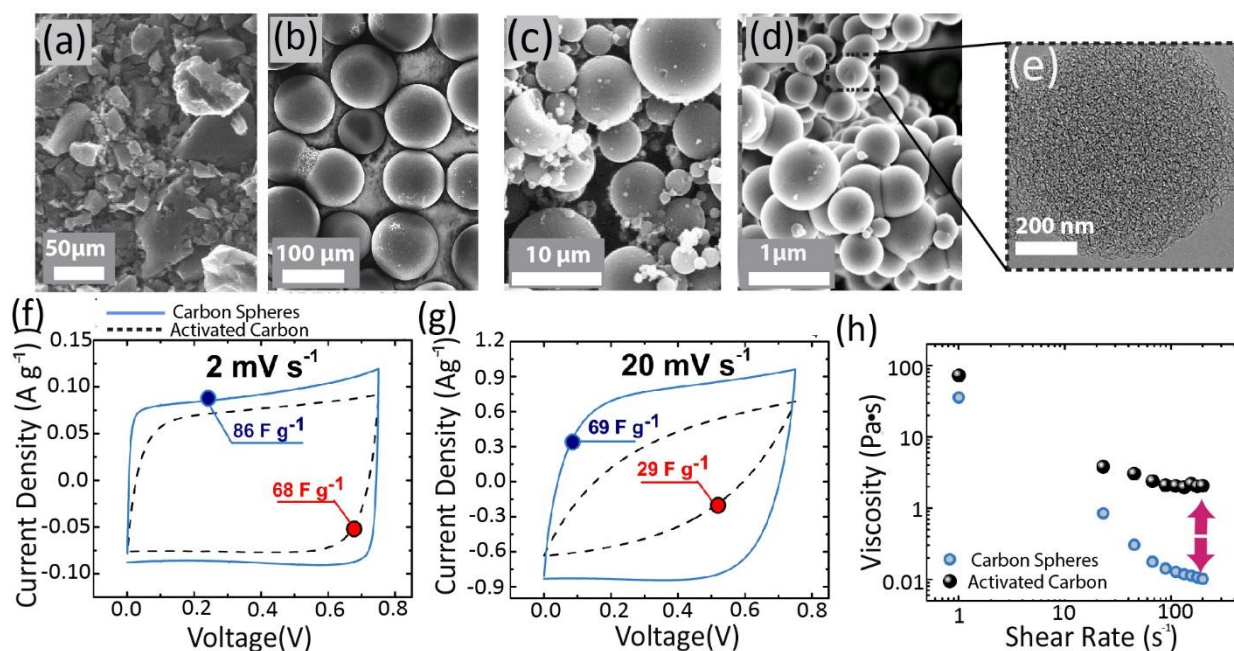


**Fig. 3.** Solid active materials studied in carbon suspension electrodes and respective electrochemical and rheological properties. SEM of anisometric activated carbon (a), activated carbon spheres derived from phenolic resin (MAST 125/250) (b) and MAST microbeads (c). SEM of Nano-carbon spheres (d) derived from an emulsion polymerization method followed by carbonization and a TEM of the material surface (e). Cyclic voltammogram at  $2\text{ mV s}^{-1}$  (f) and  $20\text{ mV s}^{-1}$  (g) for suspension composed of 20 wt% activated carbon (AC) and MAST 125-250 carbon spheres (CS) and associated shear controlled rheogram (h). Figure adapted Ref. 67, and 75 with permission from Elsevier.

RFBs are characterized by two primary storage tanks, which contain two redox-electrolytes that are circulated through the system multiple times to achieve a full charge<sup>68</sup>. In contrast, semi-solid systems are characterized by four tanks, and suspensions are charged in aliquots (finite volumes) to 100% state of charge in a single step (Fig. 2)<sup>24, 69, 70</sup>. The flow and charging protocols will be discussed in detail in section 5. The EFC utilizes high surface area materials for scalable electrostatic energy storage. As the active material flows through the anodic flow path in Fig. 2, ions adsorb onto the available surface area. Once all the accessible surface area is filled with ions, the material is fully charged. While the particles are charged, the presence of counterions and co-ions at the surface makes the particles (and suspension) electrically neutral. The EFC uses a low cost porous separator (e.g., polyvinylidene fluoride membrane), which serves to keep the two electrodes electrically separated and allows the passage of ions. In many battery systems, including flow batteries, the separator needs to be a polymer-based

**Table 1.** Porosity characteristics for various solid active materials studied in a suspension electrode. Values obtained from  $\text{N}_2$  gas sorption experiments.

Active Material	BET SSA ( $\text{m}^2\text{ g}^{-1}$ )	Average Pore Diameter (nm)	Particle Size ( $\mu\text{m}$ )	Ref
YP-50 Activated Carbon	1472	1.3	5-20	[67]
TiC-CDC	1815	1.1	2	[21]
MAST 125-250	1815	4.7	130-190	[21] [67]
MAST250-500	1341	8.6	335-440	[21] [67]
MicroMAST	1127	7.8	4.3	[67]
Nano-carbon spheres	2775	1.7	0.1-0.5	[85]
Acetylene Carbon Black	65	7.8	4-13	[21]
Amorphous $\text{MnO}_2$	192	10	-	[71]

ion-exchange membrane which introduces significant costs and maintenance to the system<sup>43</sup>.

In this section we highlight the array of the materials that have been examined for scalable electrochemical energy storage devices, specifically examining materials tested in the EFC and SSFB. Moreover, we also detail the growing emphasis on hybrid systems that take advantage of both faradic and electric double layer charge storage.

### 3.1 Electrochemical flow capacitor – electrostatic energy storage

The EFC has the advantages of both supercapacitors and flow batteries: (1) rapid charge and discharge (i.e., fast response rates and high power), and (2) decoupled energy storage and power output<sup>21</sup>. Furthermore, in comparison to other competing technologies, it may offer a long lifetime ( $\sim 100,000$  charge/discharge cycles), and a high power density ( $>10\text{ W L}^{-1}$ ) if the performance metrics of conventional supercapacitors can be achieved in the EFC. Thus, it is targeted for high-power applications on the grid<sup>5</sup>.

A suspension electrode contains an electrochemically active solid material, a conductive additive and an electrolyte which provides ions and may also provide a redox component (Fig. 1). In most cases, the active (charge-storing) material is a highly porous carbon or metal oxide<sup>71</sup>. Kastening, et al. reported the capacities of various suspension systems based on porous graphite and activated carbon with particle sizes between 10-20  $\mu\text{m}$ . The capacity of the suspensions was found to be proportional to the specific surface area of the active material and independent of particle size<sup>38</sup>. A capacity of  $150\text{ F g}^{-1}$  was achieved with the use of a high surface area activated carbon ( $1100\text{--}1500\text{ m}^2\text{ g}^{-1}$ ) suspended in sulfuric acid, while only  $3\text{ F g}^{-1}$  was observed by the graphite powder ( $8.8\text{ m}^2\text{ g}^{-1}$ ) suspension in half-cell experiments. Later, Kastening studied the charge transport mechanism in a suspension electrode due to natural or induced collision dynamics and determined that the quantity of charge transport between active particles of varying potentials was

proportional to the duration of the contact and the respective resistance between the two materials<sup>72</sup>. Both the EFC and SSFB rely on diffusion-limited aggregation of the active material and conductive additives to create pathways for electron percolation and enable efficient charge storage<sup>73, 74</sup>. Suspensions or flow-electrodes used in the EFC are strongly aggregated because the electrolyte is highly concentrated (>1 M). Porada et al., observed that the viscosity of a 10 mass% activated carbon suspension electrode in 1.0 M Na<sub>2</sub>SO<sub>4</sub> approached asymptotically 25 mPa\*s, while the same mass loading in 0.1 M Na<sub>2</sub>SO<sub>4</sub> only demonstrated about half that values ~11.5 mPa\*s. There are numerous parameters (composition, loading<sup>67</sup>, temperature, pH, solvent, surface chemistry<sup>15</sup>, etc.) that affect the rheological, electrochemical, and kinetic properties of suspension electrodes. In the following sections we detail the ongoing experimental, theoretical and computational work on suspension electrodes composed of carbon materials<sup>67, 75-77</sup>.

In an initial study, different spherical activated carbons (161-400 μm in diameter) and non-spherical titanium carbide-derived carbons (TiC-CDC) were examined as the active material for the EFC<sup>21</sup>. Under static operation using chronoamperometric methods, a capacitance of 125 F g<sup>-1</sup> (in 1 M Na<sub>2</sub>SO<sub>4</sub>) and 49 F g<sup>-1</sup> (in 1.25 M TEA-BF<sub>4</sub> in propylene carbonate) was demonstrated for a suspension containing carbon spheres (MAST 125/250) as the active material (carbon:electrolyte ratio was 1:3) (**Fig. 3b**). Since the EFC stores charge in an electric double layer at the surface of the material, it is advantageous to have a material that has a high specific surface area. Table 1 summarizes the physical properties of different materials studied in the electrochemical flow capacitor. Granular activated carbon (**Fig. 3a**) is the leading material candidate (and most studied material) currently being examined for flow electrodes utilizing electrostatic mechanisms for either ion removal from water (FCDI)<sup>13, 14</sup> or for high power grid energy storage (EFC)<sup>67, 78</sup>. Apart from granular activated carbon, a host of spherical activated carbons of varying diameters (~1-500 μm) have also been examined (**Fig. 3c and d**).

Campos et al., demonstrated that the material loading and morphology directly affect the electrochemical and rheological properties of a suspension electrode<sup>67, 79</sup>. **Fig. 3f and g** show characteristic cyclic voltammograms (CV) for a two-electrode symmetric EFC in a static test. The more rectangular the CV, the less resistive the suspension, and the more 'ideally-polarizable' is the system<sup>80</sup>. Moreover, the higher the current, the higher the capacitance, and since energy density is directly proportional to the capacitance:

$$E = \frac{1}{2} CV^2, \quad (1)$$

where  $C$  is the capacitance, and  $V$  is the voltage window, it is desirable to obtain the high currents. Spherical activated carbon spheres (MAST 125/250) (**Fig. 3b**) demonstrated better electrochemical properties than a suspension electrode composed of anisometric activated carbon (**Fig. 3a**)<sup>67</sup>. Both suspension electrodes were composed of 18 wt% active material, 2 wt% conductive additive (acetylene black) and 80 wt% 1 M NaSO<sub>4</sub>. The CS suspension exhibited a ~21% increase in capacitance (86 F g<sup>-1</sup> vs. 68 F g<sup>-1</sup>), while only experiencing a 7% greater specific surface area (1576 m<sup>2</sup> g<sup>-1</sup> vs. 1472 m<sup>2</sup> g<sup>-1</sup>) as highlighted in Table 1. The decrease in capacitance can be ascribed to inefficient utilization of the material across the thickness of the electrode. In the case of the CSs, connectivity is fairly uniform across the electrode structure. The activated carbon-based suspension electrode may experience highly random connectivity due to the formation of polydisperse agglomeration of the active material<sup>81</sup>, which can lead to large interstitial void regions and

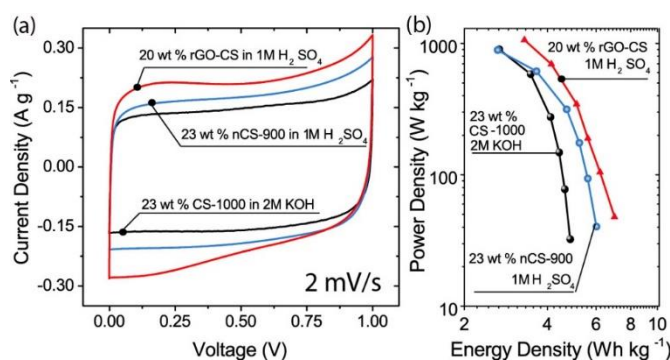


**Fig. 4.** Electrochemical properties for symmetric, all-carbon suspension electrodes. Cyclic voltammogram at 2 mV s<sup>-1</sup> (a) and Ragone plot (b) for suspension electrodes composed of activated carbon spheres (CS-1000), nano-carbon spheres (nCS), and a graphene-CS composite as active materials. Figure adapted with permissions from **Ref. 75** *The Journal of Electrochemical Society*, and **Refs. 77**, and **85** *Carbon* (Elsevier).

Table 2. Summary of physical properties of carbon active materials.

Active Material	BET SSA (m <sup>2</sup> /g)	Cumulative Pore Volume (cc/g)	Particle Size (μm)	Capacitance (F/g) @2mV/s	Ref.
CS-1000	1157	0.72	250-350	139	[75]
nCS-900	1576	0.65	0.5-1.0	154	[85]
rGO-CS	1325	0.50	125-250	200	[77]

inefficient charge percolation<sup>73, 79</sup>. At 20 mV s<sup>-1</sup> the same trend was demonstrated, between the granular activated carbon and spherical activated carbon (**Fig. 3g**). The drop in capacitance with rate was more significant for the granular activated carbon suspension electrode<sup>67</sup>.

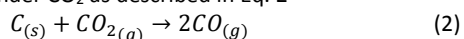
The active material morphology affects the suspension electrode viscosity (or ability to flow). Suspension electrodes composed of higher concentration (active material and/or electrolyte) demonstrate more viscous behaviors<sup>18, 67, 79</sup>. It was shown that a suspension electrode composed of the ~125 micron activated carbon spheres (2.38 Pa\*s) flowed better than suspension electrode composed of granular activated carbon (10.4 Pa\*s) at the same material loading<sup>67</sup>. Both suspensions exhibited shear thinning behavior<sup>82, 83</sup> and it was suggested that the increased viscosity seen in the granular activated carbon suspension electrode may be in part due to the strong agglomeration of the particles. These agglomerates may vary in size and hinder steady movement (flow) of the suspension due to dragging effects. Previously it has been demonstrated that suspensions with larger particles show lower viscosities than smaller particles with the same solid fraction. In addition, suspensions with more uniform size distributions and greater sphericity have shown lower viscosities than those with wide size distributions and anisometric particles<sup>84</sup>.

Much about the underlying active material arrangement ('skeleton') that forms in a suspension electrode is unknown. Recently, Cerbelaud et al, performed a numerical and experimental study on how carbon black and spherical carbons behave and form percolation thresholds in a non-aqueous solvent (propylene carbonate, PC)<sup>81</sup>. From their analysis, they suggested that nanoscale carbon black suspensions could achieve greater electron percolation at lower compositional loadings than larger spherical carbons<sup>81</sup>. They attributed this to the ease in which the material could reorganize when perturbed from a rest state. Spherical carbons have an easier time flowing, and may also easily reorganize when perturbed from a stationary state. This may have negative implications, such as a

higher percolation threshold. More experimental and theoretical work is necessary to better understand the effects of material morphology on the rheological and electro-rheological properties of a suspension electrodes.

There have been numerous studies on all-carbon suspension electrodes made of relatively cheap and abundant materials. All-carbon suspension electrodes are capable of fast charging but suffer in terms of their energy density, because they depend on the active material specific surface area for ion adsorption. To increase the energy density in an all-carbon suspension electrode, three strategies have been approached: (1) physical or chemical activation of the carbon<sup>75</sup>, (2) synthesis of highly porous nano-carbon spheres (Fig. 3d and e)<sup>85</sup>, and (3) the addition of conductive additives to suspension electrodes based on activated carbon spheres<sup>77</sup>.

The first method, physical activation, is a common approach to induce structural/physical changes in carbon and increase the surface area of the active material. Activation can occur either via chemical or physical means. A chemical or a gas can be used as a reactant with the carbon surface. Recently, Boota et al., used a physical activation under CO<sub>2</sub> as described in Eq. 2



to increase the SSA of as-received micron-sized carbon spheres from 517 m<sup>2</sup> g<sup>-1</sup> to 1157 m<sup>2</sup> g<sup>-1</sup>.<sup>75</sup> The reaction at 1000°C (1 hr) led to a nearly 50% increase in capacitance (70 F g<sup>-1</sup> to 139 F g<sup>-1</sup> at 23wt% in 2M KOH). A characteristic CV of this material in a suspension electrode is demonstrated in Fig. 4a, and labelled as CS-1000. Its subsequent rate performance is highlighted in Fig. 4b.

Given that spherical active materials are advantageous for developing efficient percolation pathways (while stationary), and for flowability, Zhang et al. demonstrated the synthesis of nano-carbon spheres (Fig. 3d and e) via an emulsion polymerization method with a resorcinol/formaldehyde mixture in the presence of alcohol and an ammonia catalyst<sup>85</sup>. The synthesized polymer spheres were then carbonized in nitrogen, and activated under CO<sub>2</sub> to produce high surface area nano-carbon spheres (nano-CSs)<sup>85</sup>. Nano-CSs, unlike the micron size CSs previously studied, offer shorter transport pathways for facile ion and charge transport, as well as a high surface area<sup>85</sup> (Table 1). The polymer (and thus carbon) spheres have tunable sizes based on synthesis time and reactant loading (resorcinol: formaldehyde ratio). The CSs activated at 600 °C in nitrogen for 6h demonstrated an amorphous structure (Fig. 3e) and a moderate to low surface area around 608 m<sup>2</sup> g<sup>-1</sup>. Nevertheless, when the nano-CSs were activated at 900 °C for 6 h their SSA increased to 1576 m<sup>2</sup> g<sup>-1</sup>, which led to a developed microporosity (Table 1) and a capacitance of 154 F g<sup>-1</sup> when tested in a suspension electrode in 1M sulfuric acid (Fig. 4a).

While high surface area microporous activated carbons are typical in the EFC, graphene and graphene oxide composite flow electrodes have also been examined as all-carbon suspension electrodes<sup>76, 77</sup>. Sasi et al, demonstrated the electrochemical behavior of a non-aqueous graphene nanoplatelet-based slurry (1.2 g graphene nanoplatelets, 20 mL of 1-butyl-1-methyl-pyrrolidinium bis(trifluoromethylsulfonyl)imide, 20 mL of propylene carbonate, 2 mL of 5 M camphor sulphonic acid, 3 mL of olyeylamin, 12 mg of

**Table 3.** Summary of half-cell and whole cell suspension electrode experiments based on intercalation chemistries.

Cathode (v/wt%)	Anode (v/wt%)	Rate	Capacity (mAh g <sup>-1</sup> ) [Thickness]	Avg. Voltage (V)	Half Cell	Ref.
LiCoO <sub>2</sub> (26 v%)		C/3.2	115 [1.4 mm]	3.75	vs. Li-metal	[19]
LiNi <sub>0.5</sub> Mn <sub>1.5</sub> O <sub>4</sub> (20 v%)		C/5	120 [1.4 mm]	4.7	vs. Li-metal	[19]
	Li <sub>4</sub> Ti <sub>5</sub> O <sub>12</sub> (25 v%)	C/3.2	170 [1.4 mm]	1.55	vs. Li-metal	[19]
LiFePO <sub>4</sub> (20 v%)	Li <sub>4</sub> Ti <sub>5</sub> O <sub>12</sub> (6 v%)	C/4	118 [1.4 mm]	~1.80		[19]
LiCoO <sub>2</sub> (20 v%)	Li <sub>4</sub> Ti <sub>5</sub> O <sub>12</sub> (10 v%)	C/8	121-134 [1.44]	2.35		[19]
LiFePO <sub>4</sub> (10 v%)	Li <sub>4</sub> Ti <sub>5</sub> O <sub>12</sub> (18 v%)	1C	140 [0.25 mm]			[24]
	Li <sub>4</sub> Ti <sub>5</sub> O <sub>12</sub> (5.7 v%)	C/5	140 [0.5 mm]	1.55	vs. Li-metal	[73]
	Li <sub>4</sub> Ti <sub>5</sub> O <sub>12</sub> (5.7 v%)	C/5	95 [1.0 mm]	1.55	vs. Li-metal	[73]
P2-type NaNCM (15 wt%)	NaTP (14.6 wt%)	0.17 mA/cm <sup>2</sup>	80 [1 mm]	1.35		[99]
	Li <sub>4</sub> Ti <sub>5</sub> O <sub>12</sub> (25 w%)	C/10	170 [1 mm]	1.6	Vs. Li-metal	[91]

sodium lauryl sulphate, and 36 mL of isopropanol)<sup>76</sup>. This suspension demonstrated 6 Wh kg<sup>-1</sup> in a flow test which was an improvement over purely graphite-based suspensions. Enhancement was attributed to the ability to form efficient 3-dimensional networks between linking graphene nanoplatelets. Boota et al, also demonstrated a similar approach making a suspension electrode of reduced graphene oxide (rGO) and micron-sized carbon spheres<sup>77</sup>. Under static conditions, the rGO-CSs demonstrated nearly 200 F g<sup>-1</sup> capacitance at 2 mV s<sup>-1</sup> (Fig. 4a). The highly conductive (connective) nature of the flow electrode contributed to good rate performances (Fig. 4b).

### 3.2 Semi-solid flow battery redox energy storage

Similar to conventional electrode systems, energy and power densities are guiding factors in developing high performing systems. Unlike conventional electrodes, suspension electrodes are limited by their flowability (rheological properties). Trade-offs that need to be considered in developing semi-solid flow battery suspension electrodes include the non-intuitive balancing of the suspension electrodes key properties: active material (w%/v%), conductive additive (w%/v%), electrolyte (w%/v%), conductivity, and viscosity. Moreover, this section highlights the importance of 'wiring' or connectivity between active materials for material utilization.

#### 3.2.1 Lithium-ion intercalation chemistries

Lithium ion intercalation materials have been extensively characterized for stationary battery applications and also studied for semi-solid batteries. Table 3 summarizes the various intercalation chemistries that have been reported in semi-solid battery systems, and highlights their key properties. Similar to stationary devices, a limiting aspect of lithium ion intercalation chemistries is the presence and growth of a solid electrolyte interface (SEI), which hinders Li<sup>+</sup> transport, and causes capacity and power fade<sup>86</sup>. A SEI layer is formed as a result of continuous solvent reduction during charging at the anode when the electrode and electrolyte first chemically reacts<sup>87</sup>. Ventosa et al., recently demonstrated that semi-solid electrodes differ significantly from static electrodes as SEI growth occurs primarily at the current collector leading to increased overpotentials during galvanostatic operation<sup>88</sup>. Solvent reduction is known to occur at low potentials (~0.8V vs. Li/Li<sup>+</sup>)<sup>19</sup>, and thus to avoid it, there has been significant efforts to utilize chemistries with high working voltages<sup>19</sup>. Material chemistries that exhibit high working

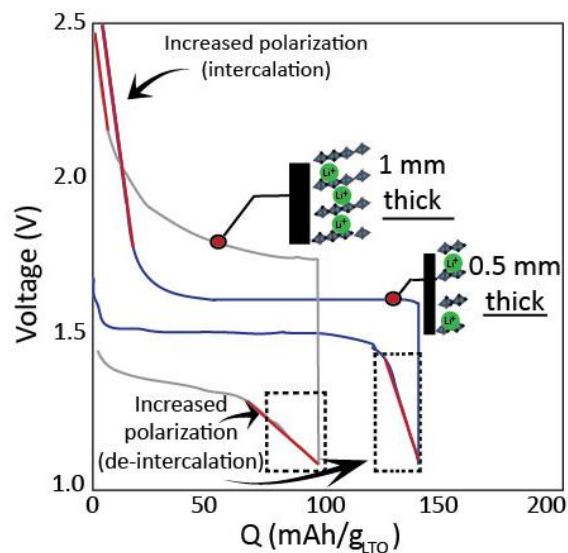


**Fig. 5.** Galvanostatic response of a LTO-based suspension electrode and effects of electrode thickness at a C/5 rate (0.5 and 1.0 mm). Suspension are 2.1 v% KB/ 5.7v% LTO suspension electrode in 1M LiTFSI-PC. Figure adapted with permission from Ref. 73. Copyright 2014, The Electrochemical Society.

(avg.) voltages are LiCoO<sub>2</sub>, LiNi<sub>0.5</sub>Mn<sub>1.5</sub>O<sub>4</sub>, and Li<sub>4</sub>Ti<sub>5</sub>O<sub>12</sub>. Of particular interest is the use of a high voltage anode such as Li<sub>4</sub>Ti<sub>5</sub>O<sub>12</sub><sup>73</sup>.

All the suspension formulations highlighted in Table 3 were studied under static conditions, and in either half or whole cell (two-electrode) experiments. The three whole-cell experiments studied include LiFePO<sub>4</sub>-Li<sub>4</sub>Ti<sub>5</sub>O<sub>12</sub> (non-aqueous<sup>19</sup> and aqueous<sup>24</sup>), and LiCoO<sub>2</sub>-Li<sub>4</sub>Ti<sub>5</sub>O<sub>12</sub> (non-aqueous<sup>19</sup>) cathode and anode pairs. Parameters such as electrode thickness, charge rate, and active material loading play a critical role in the capacity of the electrode<sup>23</sup>. Madec et al., demonstrated the implications of electrode thickness on material utilization, in a half-cell containing Li<sub>4</sub>Ti<sub>5</sub>O<sub>12</sub> based in propylene carbonate (1 M LiTFSI) (Fig. 5)<sup>73</sup>. The galvanostatic curve demonstrates similar characteristics to conventional Li<sub>4</sub>Ti<sub>5</sub>O<sub>12</sub> electrodes; namely, (1) a plateau (flat) potential, representative of a two-phase transition in Li<sub>4</sub>Ti<sub>5</sub>O<sub>12</sub>, (2) hysteresis between charging and discharging processes, (3) sloping plateau regions with

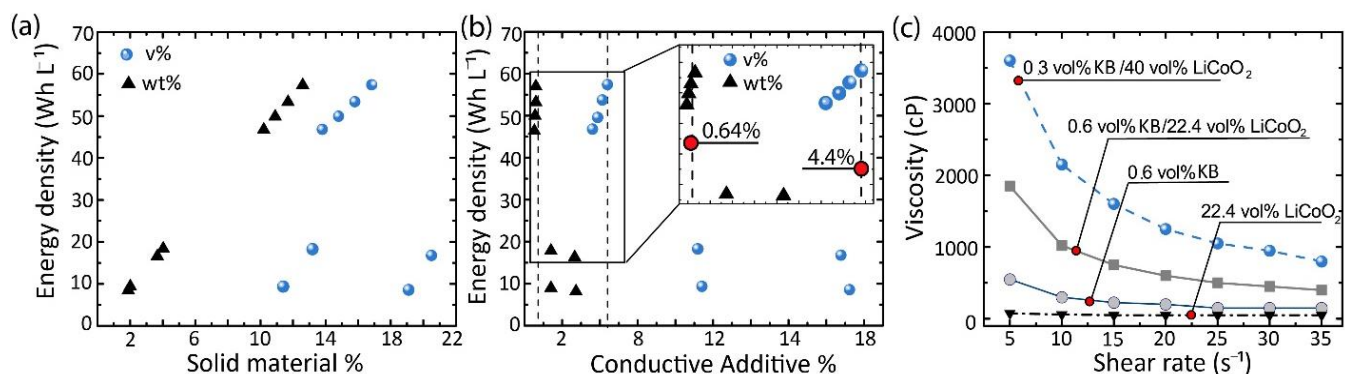


**Fig. 6.** Suspension electrode loading and its effect on energy density. Total solid material (conductive additive+active material) gravimetric (w%) and volumetric (v%) relationship to energy density in a LiFePO<sub>4</sub> (LFP)-Ketjenblack (KB) suspension electrode (a), and the effect of conductive additive w% and v% on energy density (b). Suspension electrode viscosity increases with increasing solid material loading and with the addition of KB (c) as demonstrated through shear-controlled rheological experiments. Adapted with permission from Ref. 19 *Advanced Energy Materials* and 23 *Journal of Electrochemical Society*. Copyright 2011, The Electrochemical Society.

increasing charge rate, and (4), decreasing capacity with increasing rates<sup>89,90</sup>. Suspension electrodes differ from conventional electrodes in that their galvanostatic behavior at the end of charging and discharging processes (marked in red in Fig. 5). At these two locations, the curve is linear and distinct from the plateauing region. This characteristic was attributed to increased polarization experienced at the end of the intercalation/deintercalation processes, and can be attributed to 'poor wiring' or insufficient connectivity between particles of active material<sup>73</sup>. A significant decrease in suspension electrode capacity was observed between 0.5 mm and 1.0 mm thicknesses, which can be attributed to poor connectivity. Ventosa et al, reported that the overpotential in a  $\text{Li}_4\text{Ti}_5\text{O}_{12}$  suspension electrode could be decreased through the removal of surface organic residues via  $\text{O}_2$  and  $\text{H}_2$  annealing of the active material<sup>91</sup>. This process was also shown to increase the suspension electrode's electrical conductivity two orders of magnitude from the non-treated active material<sup>91</sup>.

Optimum utilization of the active material in low conductivity metal-oxide based suspension electrodes will require careful design of the compositions<sup>92</sup>. A conductive additive is necessary to promote efficient electron percolation (and electrochemical kinetics). A common conductive additive used by the semi-solid flow battery community is Ketjenblack (KB), which is a highly conductive carbon black<sup>23, 73, 74, 79, 93</sup>. The addition of conductive additives can affect the overall energy density of a suspension electrode, and thus has to be tailored to the specific active material and electrolyte system. Hamelet et al, assessed the performance of a series of cathode suspensions composed of  $\text{LiFePO}_4$  (LFP) in 1M  $\text{LiPF}_6$ , and displayed the wide range of energy densities that can be achieved based on the compositional loading (Fig. 6)<sup>23</sup>. The energy density of a suspension electrode composed of LFP and KB scales gravimetrically with the total amount of solid material. However, from a volumetric standpoint, this trend does not hold because the KB has a low density ( $170 \text{ kg m}^{-3}$ ) in comparison to LFP ( $780 \text{ kg m}^{-3}$ )<sup>23</sup>(Fig. 6a).

When the KB wt% and v% are plotted with respect to the suspension energy density as in Fig. 6b, an optimal KB concentration emerges ( $\sim 0.64 \text{ wt}\%/4.4 \text{ v}\%$ ). A conductive additive is necessary for enabling efficient electron and charge percolation (low overpotentials), but it increases the overall suspension viscosity. Duduta et al, demonstrated that the addition of 0.6 v% KB to a 22.4 v%  $\text{LiCoO}_2$  cathode suspension resulted in an increase in the viscosity at a shear rate of  $5 \text{ sec}^{-1}$  from  $\sim 100 \text{ cP}$  to  $\sim 2000 \text{ cP}$  (Fig. 6c).<sup>19</sup> Thus, there are inherent trade-offs to creating highly conducting percolation pathways and rheological properties. To mitigate the deleterious viscous properties of adding a conductive additive Huang et al., examined a novel flow system that utilized redox shuttle molecules (ferrocene derivatives)<sup>94</sup>. In this system, tanks of LFP suspensions are held stationary and are charged and discharged by a flow system containing ferrocene and 1,1'-Dibromoferrocene, which act as redox shuttle molecules.

In a conventional system based on film electrodes, ions are free to migrate to and from the electrodes via an applied potential or current. As a result, a significant effort has been devoted to understanding the underlying active material microstructure to enhance transport properties<sup>95, 96</sup>. In contrast, in suspension electrodes, the 'flowing nature' of the suspension electrodes results to shear dynamics. These shearing dynamics can lead to loss of active material contact (connectivity), and decreases in electrical conductivity, and material utilization<sup>79</sup>.

Flowable electrodes are characterized by pseudo-insulating (electrolyte) and conducting (active material) phases. Nevertheless, electrical percolation has been shown to be as low as 1 vol% with the

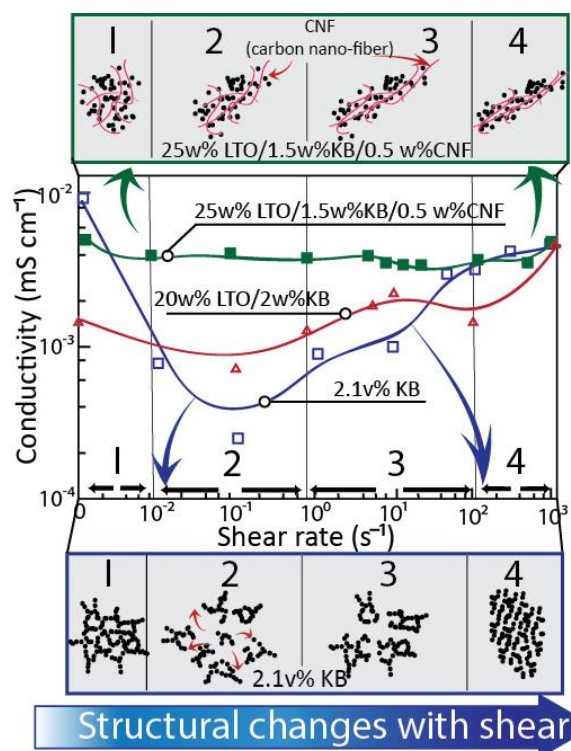


**Fig. 7.** Suspension electrode active material rearrangement during exposure to shear environments. An electrorheological plot for a suspension electrode composed of Ketjenblack (KB), KB and lithium titanate (LTO), and KB+Carbon nanofibers and LTO at an applied voltage of 100 mV. A suspension electrode composed of KB loses conductivity during shear processes because of breaking-up of active materials, however, the addition of carbon nanofibers enables constant conductivity (connectivity) with shear. Figure adapted from Ref. 79 with permission from the PCCP Owner Societies and Ref. 93 with permission from Elsevier.

use of a conducting carbon material<sup>22</sup> and is defined by a percolation threshold<sup>81</sup>. The percolation threshold is the location where electrons can freely percolate through a suspension. Youssry et al, performed a comprehensive study on how the rheological (viscosity) and electro-rheological properties of different metal-oxide and carbon-based suspensions change under the exposure to shearing (analogous to flowing) environments<sup>73, 74, 79, 93</sup>. Fig. 7 demonstrates the electro-rheological behavior of different suspension composed of KB, LTO and KB, and LTO combined with KB and carbon nanofibers<sup>79, 93</sup>. KB, and KB/LTO suspension electrodes exhibit an order of magnitude decline in electrical conductivity as a result of shearing, which can be attributed to four primary mechanisms identified on Figure 7 by numbers 1-4: (I) is a region where the agglomerates form a 3-D conducting network, (II) a region where the network breaks up, causing interstitial voids to occur, (III) formation of larger clusters which help regain conductivity, and then finally (IV) erosion into smaller more uniform particles. The mechanics of breaking up and reforming the active material network initially results in a decrease in conductivity. This rearrangement of solid materials has been mitigated by combining suspension electrodes with conducting carbon nanofibers that serve to maintain particle contact during shear. Moreover, this has also been shown to be the case when an incremental amount of surfactant is added to the suspension<sup>74</sup>. These strategies (surfactants and CNF additives) are

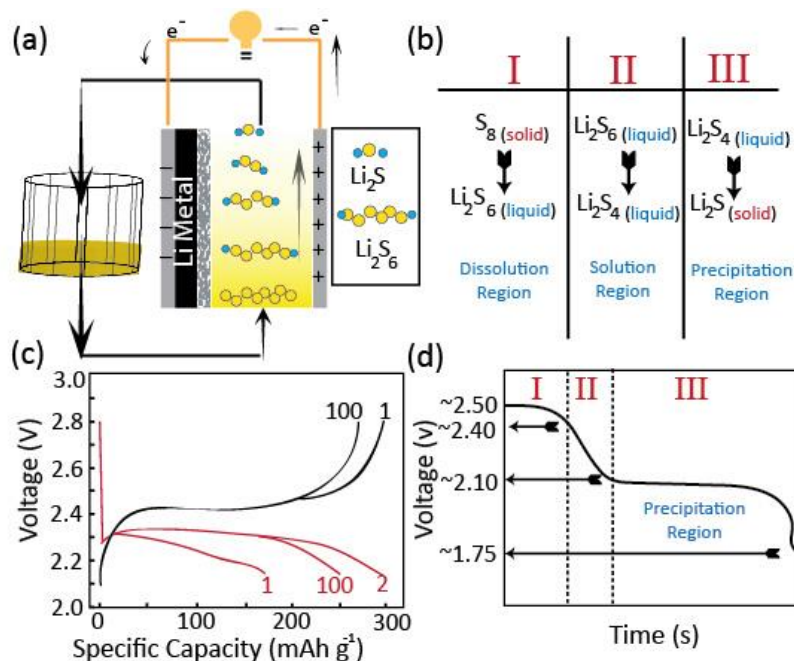


**Fig. 8.** A Lithium-polysulfide semi-liquid flow battery. Characteristic flow architecture for a semi-liquid polysulfide cathode utilizing sulfur to  $\text{Li}_2\text{S}_4$  discharge products (a) and summary of different polysulfide products that result during discharge and their active state (solid or liquid) (b). A voltage profile of a 5M  $\text{Li}_2\text{S}_8$  catholyte charged and discharged at 0.8 C at different cycle numbers (c) and breakdown of voltage curve by reaction products (d). Figure adapted from Ref. 102 with permission from The Royal Society of Chemistry

strategies to maintain connectivity between active material particles during shearing<sup>74,93</sup>. While electrochemical and electro-rheological methods have been utilized to characterize active material arrangement, the actual change in morphology with shearing, has yet to be visually observed. In-situ techniques that can visualize the material arrangement in a charging suspension electrode during shearing processes are necessary for better design of flow-electrodes.

### 3.2.2 Sodium-ion semi-solid flow battery

While lithium ion batteries are widely used, limited supply of lithium justifies exploration of alternative material chemistries based on low-cost and abundant ions such as sodium are growing in interest especially in large-scale applications. Examples of chemistries currently being explored in 'solid' stationary devices include sodium-sulfur, sodium-air, and sodium-ion and hybrid Na/Li-ion cells<sup>9, 97, 98</sup>. Recently a non-aqueous SSFB based on a Na-ion chemistry was proposed by Ventosa et al.<sup>99</sup> Similar to the previously described lithium intercalation compounds, Na-ion systems rely on intercalating crystalline material chemistries for energy storage. Ventosa et al, demonstrated the concept of a Na-ion SSFB containing a P2-type  $\text{Na}_x\text{Ni}_{0.22}\text{Co}_{0.11}\text{Mn}_{0.66}\text{O}_4$  (NaNCM) suspension cathode, and  $\text{NaTi}_2(\text{PO}_4)_3$  (NATP) suspension anode<sup>99</sup> (Table 3). NATP is a commonly explored NASICON material for Na-ion anodes, which displays a theoretical energy density of  $133 \text{ mAh g}^{-1}$ , while NaNCM has displayed similar capacity of  $130 \text{ mAh g}^{-1}$ .<sup>100</sup> In a SSFB, these materials demonstrated a reversible specific charge capacity of  $80 \text{ mAh g}_{\text{cathode}}^{-1}$ , with an energy density ca,  $9 \text{ Wh L}^{-1}$ . The major limitations of suspension electrodes, as mentioned previously, are the large and inherent overpotentials, which limits the full voltage window to 2.2V (rather than 2.5 V)<sup>99</sup>. Growing challenges among all suspension electrode systems is understanding how the active material, electrolyte, and conductive additives can be designed to

decrease these overpotentials (thereby increasing the accessible voltage window), without sacrificing coulombic efficiency.

### 3.2.3. Polymer-redox flow batteries

Several polymer based chemistries have been studied in a suspension based electrode. A Zn/PANi system was examined with Zn as the anode (and host for Zn plating) and a suspension made of PANi particles as the cathode. The whole cell performance reached nearly  $112 \text{ mAh g}^{-1}$  after 30+ cycles<sup>53</sup>. This system was significantly improved through the use of Ag doped PANi which led to greater coulombic efficiencies<sup>54</sup>. Finally, a polypyrrole microparticle suspension was also studied in the presence of manganese sulfate. This system takes advantage of the multiple oxidation states of manganese (Mn (II), Mn(III), and Mn (IV)), via utilizing electrodeposition processes at a stationary carbon anode.

### 3.2.4. Lithium-sulfur (Precipitation-dissolution chemistries)

Recently, a semi-liquid lithium/polysulfide (Li/PS) battery was introduced for grid energy storage. Unlike other lithium chemistries based on insertion cathode materials (as discussed earlier), lithium-sulfur batteries undergo precipitation-dissolution reactions (Fig. 8a)<sup>101</sup>. Materials based on intercalation chemistries undergo a phase change, while sulfur compounds undergo a transformation from a solid (sulfur) to a liquid (lithium polysulfides) during charging (Fig. 8b and d). Yang et al. showed that Li/PS batteries could be used for scalable flow systems if a limited voltage window was utilized.<sup>102</sup> A catholyte composed of  $\text{Li}_2\text{S}_8$  in an ether solvent remains in the solution region as long as it is cycled between sulfur (2.8 V) and  $\text{Li}_2\text{S}_4$  (~2.2V) (regions I and II in Fig. 8b and d)<sup>102</sup>. This voltage window completely avoids the precipitation region III of the discharge curve and utilizes the high solubility of long-chain polysulfides for flowable energy storage (Fig. 8a). The catholyte in these experiments was a lithium polysulfide ( $\text{Li}_2\text{S}_8$ ) suspension in 1,3 dioxolane (DOL), 1,2-dimethoxyethane (DME), which was paired with a stationary Li-metal

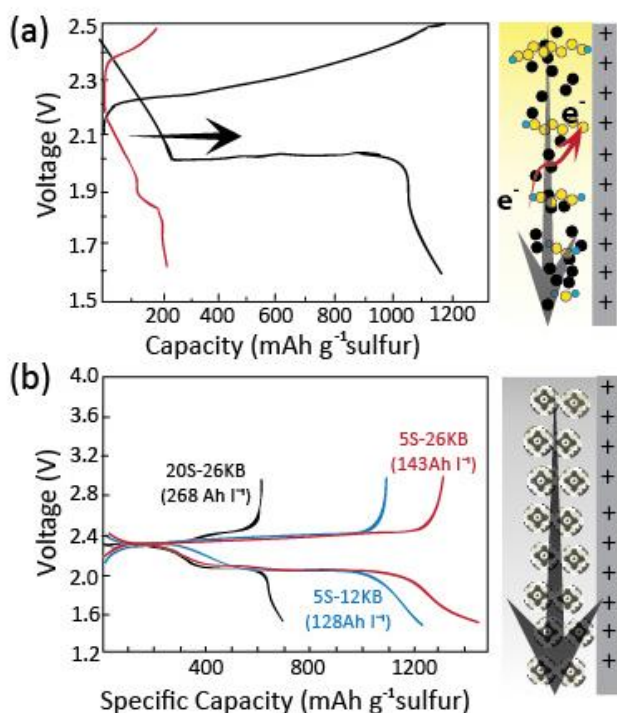


**Fig. 9.** A Lithium-polysulfide semi-solid flow battery based on conducting carbon networks. Galvanostatic curve of a Li/PS battery based on a typical carbon fiber electrode and the increased capacity achieved when a 3-dimensional flowable carbon network formed of Ketjen black was used (a). An extension of the voltage window can be achieved with the use of a semi-solid Li/PS battery composed of sulfur impregnated in carbon black. Figure adapted from Ref. 22 and 107. Adapted with permission from Ref. 22. Copyright 2014, American Chemical Society and from Macmillan Publishers Ltd: *Nature Communication* Ref. 109, copyright 2015.

anode. At 0.8C C-rate a 5 M  $\text{Li}_2\text{S}_8$  catholyte achieved a capacity of 334  $\text{mA h g}^{-1}$  (Fig. 8c) and energy densities of 95  $\text{Wh kg}^{-1}$ /106  $\text{Wh L}^{-1}$ . Eliminating the precipitation phase (region III) is expected to increase the cycle life significantly, because the precipitation region is known to cause irreversible loss of sulfur as  $\text{Li}_2\text{S}_2/\text{Li}_2\text{S}$  products deposit on the anode and cathode. This mechanism decreases the coulombic efficiency, lowers the capacity, and increases the cell impedance<sup>103, 104</sup>. Fan et al. recently examined the electrodeposition kinetics of  $\text{Li}_2\text{S}$  in glyme solutions onto carbon fiber and multiwalled carbon nanotubes. It was shown precipitation and subsequent growth occurs preferentially at three-phase boundaries (electrolyte|substrate| $\text{Li}_2\text{S}$ ) and requires and 100 mV overpotential for nucleation<sup>105</sup>. Future work is needed to understand the reversibility of this process in order to design long-lasting materials.

The capacity and energy density can be increased further by increasing the concentration of the suspension or altering the solvent<sup>106</sup>. While RFBs are limited to concentrations of ~1.7-2 M due to stability issues<sup>41</sup>, Li/PS solutions approach concentrations close to 7 M in DOL/DME and 10 M in tetrahydrofuran<sup>107</sup>.

Fan et al. combined a Li/PS solution with a flowable conductor network of nano-carbon materials to increase reaction sites throughout the volume of the flow-electrode<sup>22</sup>. Fig. 9a compares Li/PS catholytes based on a stationary carbon fiber current collector and a flowable conducting nano-carbon network ('liquid-wire')<sup>108</sup>. The cathode suspension contained 2.5 mol S/L in TEGDME with 1 wt%  $\text{LiNO}_3$  and 0.5M LITFSI. In typical flow-battery systems based on

stationary current collectors, the reactions are limited to the region adjacent to the planar current collector (typically a carbon fiber or carbon felt). By adding conductor particles directly to the polysulfide solutions, there is a greater volume for electrochemical reactivity beyond the current collector. This extension of the electrochemically active region contributes to a 5x higher capacity when compared to the Li/PS battery based on a stationary carbon fiber current collector (Fig. 9a). The addition of 1.5 v% of KB led to a 1200  $\text{mAh g}^{-1}$  capacity at a C/4 rate. The increase in capacity when compared to the pure lithium polysulfide solutions (Fig. 8c) can also be attributed to the extension of the voltage window into the precipitation region. Thus, the addition of conducting networks to polysulfide solutions enables greater utilization the material, as well as good coulombic efficiencies (>95%) into the precipitation region. This concept was expanded by impregnating a mesoporous carbon with sulfur as the active material in a semi-solid polysulfide battery (Fig. 9b)<sup>109</sup>. Through this design, a maximum energy density can be achieved, as each part of the discharge curve (I, II, and III) can be accessed. Having carbon impregnated with solid sulfur allows region I to be fully utilized and a discharge capacity well above 1200  $\text{mAh g}^{-1}$ <sup>109</sup>.

### 3.3 Hybrid approaches toward increasing the energy density in suspension electrodes

The all-carbon suspension electrodes described in the electrochemical flow capacitor section exhibit high power density, but are limited in terms of their energy density. In order to increase the energy density, one can either increase the voltage window or the active material's capacitance. For suspensions based in aqueous electrolytes, the voltage window is thermodynamically limited to approximately 1.2 V because water decomposition occurs above 1.23 V<sup>59, 110, 111</sup>. Pseudocapacitors (or redox electrochemical capacitors) and hybrid devices are two avenues toward increasing the energy density. In this section we focus on three approaches toward achieving a high-capacity carbon-based suspension. These methods include the use of (1) soluble carbonyl-based organic molecules with a carbon suspension (pseudocapacitor), (2) asymmetric device AC/metal oxide hybrid systems, and (3) soluble metal redox couples combined with carbon suspensions (pseudocapacitor) or a "suspension redox flow battery". The latter opens the door for a new area of study toward novel electrodeposition battery systems.

#### 3.3.1. Carbonyl-group containing organic molecules as redox mediators

Insulating organic RFBs have garnered significant attention in the last couple of years, because carbonyl-based organic molecules (C-bOMs) are low cost, abundant, and offer tunable properties<sup>112-114</sup>. But beyond RFB applications C-bOMs can be used to increase the capacitance in non-aqueous and aqueous carbon-based energy storage devices through the addition of fast and reversible redox reactions at the electrode|electrolyte interface (Fig. 10a). These C-bOMs can either be grafted on the surface of the electrode<sup>115-118</sup> or dissolved producing a redox-active electrolyte<sup>20, 119-121</sup>. The majority component in a suspension electrodes is the electrolyte, thus making the electrolyte a source for additional capacitance (Faradic reactions) could provide a significant contribution to the total energy stored by the system.

Hydroquinone<sup>119, 121</sup>, indigo carmine<sup>122</sup>, p-phenylenediamine (PPD)<sup>123</sup>, and m-phenylenediamine<sup>124</sup> are just a few examples of organic compounds explored as C-bOMs for redox-active electrolytes in conventional electrochemical capacitors. Recently, hydroquinone and p-phenylenediamine were explored in suspension electrodes composed of microporous carbon spheres<sup>20, 121, 125</sup>. A suspension

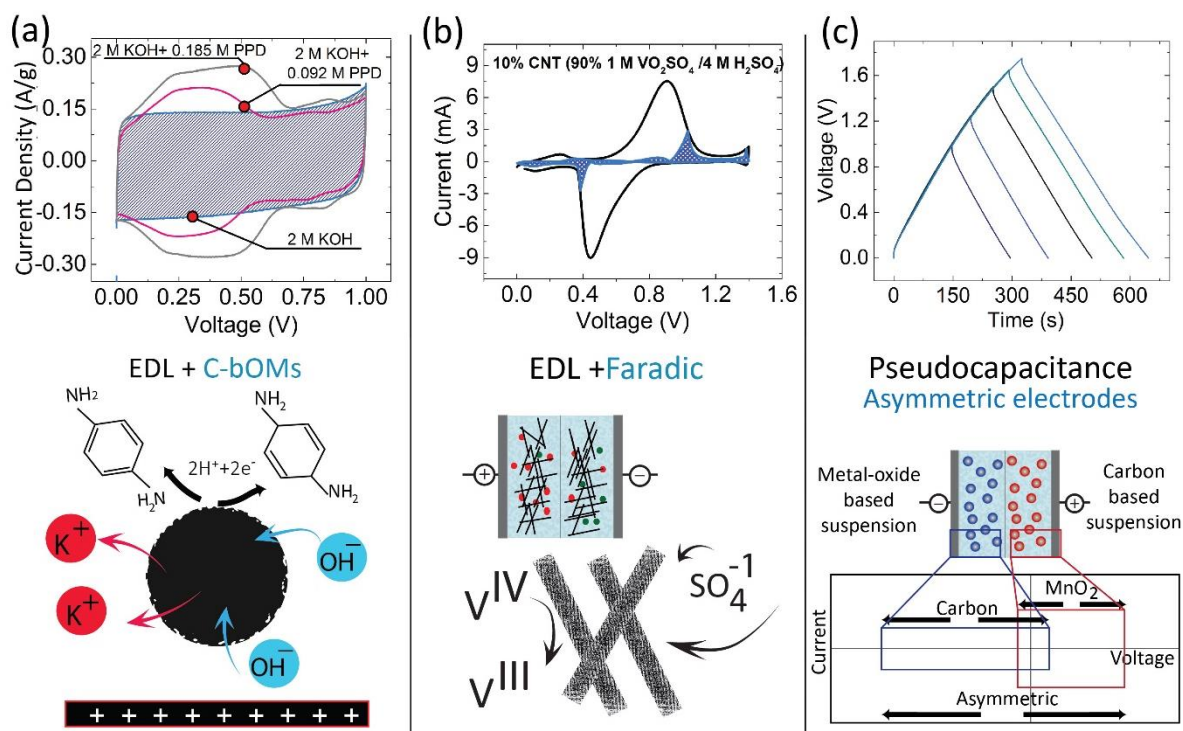


**Fig. 10.** Hybrid approaches for improving the energy density in all-carbon based suspension electrodes. P-phenylenediamine used as a redox-mediator in a basic solution (2M KOH), adds additional charge storage to an electrostatic carbon-based suspension. Redox peaks are observed by suspension electrodes based in 2 M KOH with the redox mediator (a). Apart from organics, metal-based redox-active electrolytes can be used for additional charge storage. The combination of  $\sim 10$  wt% multi-walled carbon nanotubes in a 1M  $\text{VO}_2\text{SO}_4/4\text{M H}_2\text{SO}_4$  electrolyte demonstrates defined redox peaks. The shaded region is an estimation of surface (electrostatic) charge storage, while the remaining area of the CV is faradic charge storage related to the  $\text{VO}_2^+/\text{VO}^{2+}$  redox couple (b). An asymmetric design with a  $\text{MnO}_2$  cathode and an activated carbon anode can achieve an  $\sim 1.7$  V voltage window a neutral aqueous (1 M  $\text{Na}_2\text{SO}_4$ ) electrolyte, due to the fact that each electrode occupies a different voltage region (c). Figure adapted with permission from **Ref. 20** from Elsevier, **Ref. 6**. Copyright 2015, The Electrochemical Society, and **Ref. 71** Copyright 2014, American Chemical Society.

composed of 23 wt% activated carbon spheres (**Fig. 3b**) with different concentrations of PPD dissolved in potassium hydroxide (2M KOH) demonstrates visible redox peaks with heights proportional to the concentration of C-bOMs (**Fig. 10a**). In general, soluble C-bOMs undergo proton-coupled electron transfer (PCET) reactions at the electrode interface, which contributes to additional charge storage. PPD undergoes a standard two-proton/two-electron oxidation and reduction reaction between p-phenylenediamine and p-phenylenediamine, which is observed in the characteristic redox peak at 0.4 V<sup>20</sup> (**Fig. 10a**). The rectangular hatched region is a case with no redox mediator added, and thus energy stored is primarily through electrostatic means (**Fig. 10a**). At 2 mV s<sup>-1</sup>, the addition of PPD increased the energy density from 118 F g<sup>-1</sup> to nearly 220 F g<sup>-1</sup><sup>20</sup>. Boota et al., were further able to increase the capacitance (and subsequent energy density) through the use of hydroquinone in acidic medium (sulfuric acid), demonstrating nearly 342 F g<sup>-1</sup>. Carbonyl-based organic molecules used as redox active electrolytes combined with carbon-based suspension electrodes enable enhanced capacitances and energy densities. Their demonstration in carbon suspension electrodes based on non-aqueous electrolytes has yet to be achieved, but could offer even higher energy densities, due to an inherently larger voltage window.

### 3.3.2 Soluble metal redox couples and electrodeposition batteries

Carbon-based suspension electrodes can serve as a host for electrostatic energy storage as well as a substrate for faradic reactions. Recently, this concept of flowing current collectors was demonstrated as a means to hybridize the electrochemical flow

capacitor with redox electrolytes containing the  $\text{VO}_2^+/\text{VO}^{2+}$  metal-based redox couple (**Fig. 10b**)<sup>6</sup>. When a suspension composed of 10 wt% carbon nanotubes was combined with a mixed electrolyte (1M  $\text{VO}_2\text{SO}_4/4\text{M H}_2\text{SO}_4$ ) characteristic redox peaks are observed in the cyclic voltammogram. The blue hatched region in the cyclic voltammogram is the energy stored via electrostatic means, while the remaining area between the curves is proportional to the energy stored via faradic means<sup>6</sup>. The contributions from ion adsorption mechanisms are low because carbon nanotubes demonstrated a low specific surface areas (<500 m<sup>2</sup> g<sup>-1</sup>). Thus, it has been shown that the EFC can be used in combination with metal redox species for both faradic and capacitive energy storage.

Beyond soluble metal redox couples, this concept (combining metal redox species and carbon substrates) can be expanded to include commonly known and characterized chemistries based on electroplating principles, such as the zinc-air battery. The zinc-air rechargeable battery, relies on the formation of ZnO and subsequent reduction to metallic zinc during charging<sup>126</sup>. Nevertheless, these electroplating systems are fundamentally hindered in terms of lifetime because of irreversible loss of material during cycling, and degradation due to dendrite formation. If these two factors could be mitigated (via electroplating onto carbon substrates or in the pores), a larger materials inventory could be accessed. Examples of low cost and abundant elements that could be used include zinc, manganese, copper, sulfur and iron. All of these elements, in different oxidation states have the ability to plate. Recently, a zinc-polyiodide chemistry was introduced as a high energy density (167 Wh L<sup>-1</sup>) RFB<sup>49</sup>.

Nevertheless, one of limiting aspects, is finding methods to ameliorate zinc dendrite growth. This concept, utilizing flowable carbon substrates for electroplating, has been demonstrated by Savinell's group for an all-iron flow battery<sup>127</sup>.

### 3.3.3 Asymmetric activated carbon/MnO<sub>2</sub> suspension systems

Finally, the energy density in carbon-based suspension systems can be improved through an expansion of the voltage window. The voltage window can be increased by using non-aqueous (2-3V)<sup>85</sup> or ionic liquid (2-4V)<sup>85</sup> electrolytes. Nevertheless, these working electrolytes are both costly, and require the use of an inert atmosphere, which leads to greater complexity in large-scale systems. In contrast, an expanded voltage window can be achieved in neutral aqueous solutions through an asymmetric electrode design. In this scenario, one electrode is comprised of a battery-type faradic electrode (cathode) and the other is a capacitive-type electrode (anode). In a mass-balanced system, the voltage window can be expanded as the potential window for each electrodes is accessed (Fig. 10c). Specifically, MnO<sub>2</sub> can be polarized more positively without O<sub>2</sub> evolution due to the reduction of Mn (IV) to Mn (III) at the cathode surface<sup>110</sup>. Moreover the anode (carbon-based electrode) can be polarized more negatively, because the microporous network of the activated carbon serves as a substrate for adsorbing evolved atomic hydrogen. Thus, by balancing the masses of each electrodes in respect to their associated capacitance, an extended voltage window and thus a higher energy density can be achieved. Recently it was demonstrated that this could be an effective method for increasing the voltage window in an AC/MnO<sub>2</sub> based EFC to ~1.7V in 1 M NaSO<sub>4</sub> (Fig. 10c)<sup>71</sup>. The asymmetric design reached near 11 Wh kg<sup>-1</sup> (at 50 W kg<sup>-1</sup> power density).

## 4. Suspension electrodes for energy generation and water treatment technologies

While the prior sections emphasized materials in suspension electrodes for grid energy storage, there is also growing interest in suspension electrodes for water treatment, deionization, and generating renewable energy. Just as the electrical grid is in need of rebuilding in order to meet intermittent energy demands and accommodate renewable energy resources, critical water infrastructures are also facing a similar challenge due primarily to rising populations, and climate change. The following section interprets recent efforts to develop scalable and versatile systems for ion removal<sup>13-18, 128</sup>, renewable energy generation<sup>18, 129</sup>, and for wastewater treatment<sup>26-28</sup>.

### 4.1 Capacitive deionization – brackish and unconventional water treatment

Brackish and point-of-use water treatment is a growing area, as it is abundant and easier to treat (deionize) than seawater. While reverse osmosis and membrane distillation methods are the primary methods utilized to treat brackish waters, capacitive deionization (CDI) is becoming preferred<sup>130-132</sup>. Since CDI removes ions from solutions it is targeted for deionization of low-concentration solutions, compared to membrane processes that extract water from brine. In conventional CDI systems, two stationary film electrodes are placed in parallel similar to Fig. 11a, and a feed water stream flows parallel to each electrode. When a potential is applied between the electrodes, ions adsorb into the surface of the electrode, and the concentration and effluent is decreased. As the film electrode becomes saturated with ions, it reaches a point where ion removal must commence, and the electrodes are regenerated with an applied 0V (or voltage reversal process). This process results in a fluctuation in the effluent concentration, and requires an intermittent

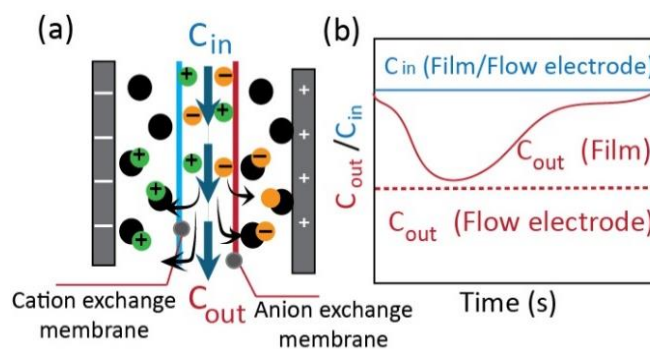


**Fig. 11.** A schematic of flow capacitive deionization (FCDI), in which two suspensions flow through external channels against parallel current collectors, and ions are removed from feedwater stream that runs through a center channel (a). For a constant feedwater input concentration, the effluent concentration remains constant in FCDI, whereas CDI based on film electrodes experiences a saturation point, and fluctuating effluent concentrations (b). Figure adapted from Ref. 16 with permissions from Elsevier.

operational mode (Fig. 11b). In contrast, in membrane based FCDI, there are two external channels that flow carbon-based suspension electrodes, and a middle channel in which feed water flows. In operation, the three channels run in parallel and cations traverse a cation exchange membrane, and anions migrate across an anion exchange membrane as a result of an applied potential (Fig. 11a). Once the ions enter the flow-electrode channel, they can adsorb onto the surface of the active material (activated carbon) in an electric double layer and the effluent from the feed water channel is a lower concentration solution. FCDI (in contrast to CDI) can achieve a constant effluent concentration which enables more versatile operational modes, and electrodes with higher ion removal capacities<sup>16</sup> (Fig. 11b). This higher capacities may enable the use of FCDI in higher concentration solutions, where typical CDI is limited. Research efforts within FCDI have primarily focused on evaluating the system performance with different feed solutions<sup>13, 14</sup>, operating potentials<sup>18</sup>, and carbon loadings<sup>15, 18</sup>. Moreover, it has been reported that material surface chemistry affects suspension viscosity and thus plays a role in the pumping and energy consumption by a FCDI system<sup>15</sup>. For FCDI to be competitive with current technologies, the energy consumption of operating flow-electrodes must be decreased and energy recovery increased.

#### 4.1.1. FCDI – active material surface chemistry and energy recovery

One of the main motivations for FCDI is its opportunity for low energy consumption and the potential for energy recovery. FCDI brings an additional ancillary energy consuming process (pumping) which must be taken into consideration. Energy recovery is also more difficult, as the electrodes have greater susceptibility to parasitic losses due to both the dynamic nature of the operation, and increased resistances (leakage current). To minimize high system resistances and subsequent energy loss a zero-gap architecture was proposed<sup>16</sup>. In a zero-gap electrode, the feedwater channel is removed, and instead is directly combined with adjacent flow-electrodes. In membrane-based FCDI it has been shown that the energy can be recovered more efficiently when flow-electrodes were discharged in deionized water instead of a salt solution. When deionization occurred at 1.2V, approximately 26% of the energy inputted for ion removal was recovered<sup>14</sup>. Gendel et al. demonstrated a continuous a process for ion removal and energy recovery through the use of two parallel reactors<sup>17</sup>. Later

Rommerskirchen et al. proposed an alternative architecture with a single module (with a split feedwater channel) and a single flow electrode. A split feed water channel enabled water recoveries of ~80% and minimized the energy costs associated with pumping two flow-electrodes<sup>133</sup>. Nevertheless, one continuous flow-electrode dampens opportunities for energy recovery.

The active material plays a role in the salt removal efficiency and the energy consumption of a system. Fig. 12a shows an XPS plot of an anisometric activated carbon (as-received), and an activated carbon (AC) that has been lightly oxidized with nitric acid. It has been shown that the oxidation of the carbon significantly impacts the flowability. An electrode composed of 20 wt% activated carbon flows similarly to that of a flow-electrode composed of 28wt% oxidized AC<sup>15</sup>(Fig. 12b). This decrease in viscosity (via active material modification) led to a decrease in the pumping energy by nearly 5x. Nevertheless, the oxidized material demonstrated greater resistances and deionization voltages (Fig. 12c). During constant current operational mode, it was shown that it requires a higher operating voltage to remove 18% of the ions from the feed water solution, for the flow electrode based on oxidized AC (Fig. 12c). Thus, active material surface chemistry plays a role in the salt removal, and electrical and pumping energy consumption. More synergistic material design may enable highly flowable and energy efficient flow-systems.

#### 4.1.2 FCDI– effect of feed water concentration and active material loading

Initial work with FCDI evaluated the new electrode architectures ability to treat all types of water (e.g. brackish and seawater)<sup>13</sup>. It has been observed that salt removal efficiency substantially increases from 12.4% to 61% as the feed water concentration is decreased from seawater (35 g/l) to brackish waters (0.2 g/l) while the applied potential remained fixed at 1.2 V<sup>13</sup>. This suggests that FCDI, similarly to conventional CDI, may be best for the treatment of low concentration solutions. Additionally, another approach without membranes was also tested in high concentration solutions and salt removal efficiencies approached 7.3% at a much lower applied potential of 0.5 V<sup>16</sup>. The lower salt removal rate is consistent with the lower rates observed with CDI versus membrane based CDI<sup>13, 130, 131</sup>. The salt removal efficiency can be calculated using equation

$$E(\%) = \left(1 - \frac{c_{\text{salt,out}}(t)}{c_{\text{salt,in}}}\right) \times 100, \quad (2)$$

where  $c_{\text{salt,out}}$  and  $c_{\text{salt,in}}$  are the concentration of salt at the inlet and exit of the CDI cell. In their initial studies, Jeon et al. demonstrated that the salt removal efficiency decreased with feed water concentration and the salt removal rate increased from 0.029 to 0.977 mmol/m<sup>2</sup>s as the feed water concentration increased from 0.2 g/L to 35 g/L. The salt removal efficiency increased with feed water concentration due to a decrease in ohmic resistance which can lead to higher current densities (higher salt fluxes). The salt removal rate is calculated as:

$$J_{\text{salt}} = -\frac{L\Phi}{A} \frac{(c_{\text{salt,out}} - c_{\text{salt,in}})}{dz}, \quad (3)$$

where  $L$  is the channel length, is the flow rate,  $A$  is the membrane area, and  $dz$  is the distance along the channel.

Most FCDI system have utilized suspension electrodes with low carbon loadings (e.g., 5 wt%) primarily because pumping energy (and clogging) concerns outweigh system performance at this initial stage of testing. However, as the carbon loading of flow-electrodes is increased from 10 wt% to 25 wt% the salt removal rate was shown to increase ~0.05 to 0.25 mmol/m<sup>2</sup>/s<sup>18</sup>. Continuous long term

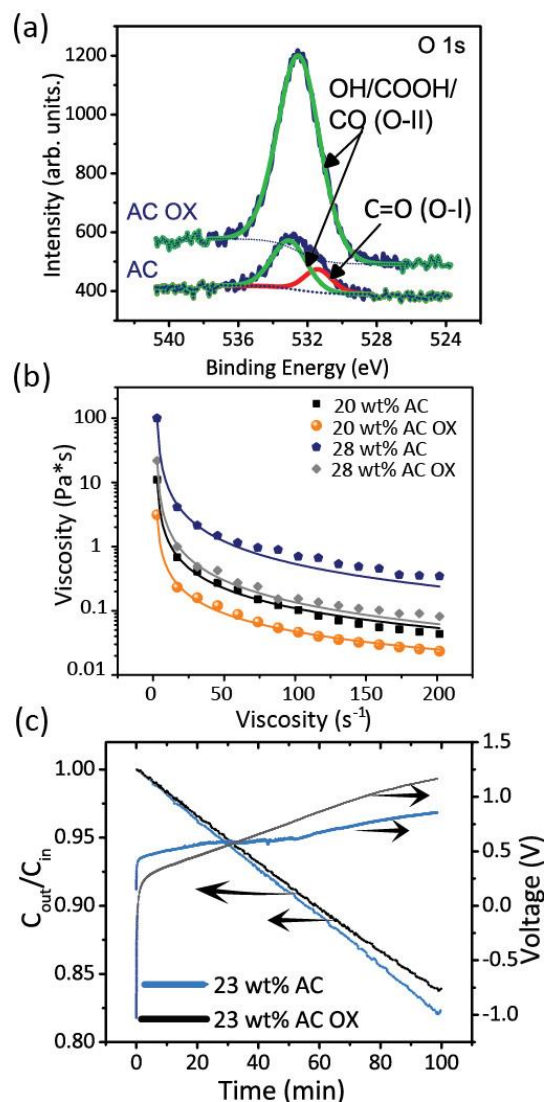
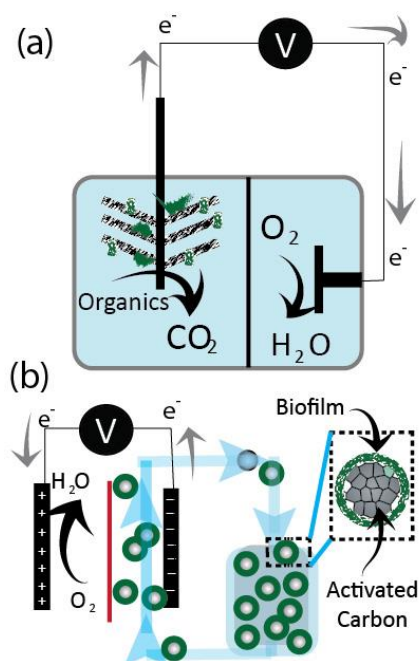


Fig. 12. XPS of activated carbon (AC) and AC oxidized with nitric acid. The oxidized and as-received carbons was studied as the active material in a suspension electrodes. A rheogram for different flow-electrodes composed of varying carbon loadings (b) and Ion removal properties for suspension electrodes composed of 23 wt% AC and 23 wt% oxidized AC at a constant current (30 A/m<sup>2</sup>) (c). Adapted with permission from Ref. 15. Copyright 2015, American Chemical Society

operation of 25 wt% flow electrodes is difficult as clogging and membrane scaling is may occur.

#### 4.2 Capacitive mixing – salinity gradient energy

Nearly 2.6 TW of energy is currently being released through the mixing of seawater and river water at global estuaries. Three technologies currently being investigated as a means for capturing this energy are pressure retarded osmosis, reverse electrodialysis and capacitive mixing. The latter of these three technologies is in its early stage of development, and relies on generating energy through reversibility expanding and compressing the electric double layer at the surface of an electrode, as the electrode is exposed to river and seawater solutions. Alternatively if membranes are coated on the capacitive electrodes, energy is generated by reversing the whole cell Donnan potential as river and seawater approach the electrodes.



**Fig. 12.** Microbial fuel cells utilized in energy recovery from wastewater (a), and a scalable MFC based on carbon-biofilm based suspension electrode (b).

This EDL or Donnan process however, cannot occur simultaneously with a fixed electrode architecture, which results in intermittent energy generation. Two approaches based around reversing FCDI have recently been employed to generate energy continuously. The first approach utilized one reactor to create a concentration gradient between a flow electrode (10% AC in 0.6 M NaCl electrolyte) and feed water stream (17 mM NaCl electrolyte) membrane interface<sup>18</sup>. This concentration gradient across each membrane generated a whole cell voltage for energy generation. Peak power densities approached that obtained with fixed film electrodes ( $\sim 30 \text{ mW m}^{-2}$ ). A second approach utilized a four reactor system where the flow-electrodes were able to undergo the typical four step capacitive mixing process in separate reactors. This approach allows for continuous recycling of the flow-electrode because the active material is charged and discharged during a complete cycle. Therefore a fixed volume of suspension electrodes could in theory operate infinitely and generate energy continuously<sup>25</sup>.

#### 4.3 Microbial Electrochemical Technologies - Wastewater treatment

There is a need for new and innovative technologies that are capable of harvesting energy from organic matter in domestic wastewater streams. It has been estimated that nearly 2 kWh of energy is available in each cubic meter of wastewater<sup>134, 135</sup>, which represents nearly  $1.5 \times 10^5$  GWh of energy yearly in the United States<sup>4</sup>. Anaerobic digestion represents a leading effort to harvest this energy using methanogenic bacteria to convert organics to methane and carbon dioxide. This methane can be converted to electricity at the expense of energy conversion losses. Microbial electrochemical technologies (METs), alternatively aim to directly convert organic matter to electricity and carbon dioxide<sup>136</sup>. METs use exoelectrogenic bacteria which respire (oxidize) organic matter under anaerobic conditions, and are capable of releasing electrons onto a solid conducting surfaces<sup>4</sup>. This anodic response can be coupled to various cathodic reactions to promote either hydrogen or

electricity production. One of the major hurdles with scaling METs has been the limited surface area available for biofilm growth, and electron release. High surface area brush electrodes<sup>137</sup> are utilized in lab scale systems, yet scaling brush electrodes results in the need for large reactor volumes which often suffer from high ohmic losses<sup>138</sup>. Therefore in terms of both, wastewater treatment and energy production, increasing the anolyte to reactor volume in METs is paramount.

Efforts to mitigate this dependence on fixed solid biofilm growth substrates (graphite brushes) in METs recently employed a suspension electrode comprised of a biofilm laden granular activated carbon particles as the anode, coupled to a fixed-film oxygen reduction cathode.<sup>27</sup> Granular activated carbon was chosen based on the high surface area, rough surface, and electron conducting properties. All of these characteristics promoted sufficient biofilm adhesion<sup>139</sup>. The suspended granular activated carbon biofilm anode showed similar performance to fixed non-suspension based anodes in terms of power ( $\sim 1000 \text{ mW m}^{-2}$ ) and coulombic efficiencies ( $\sim 50\%$ ), but resulted in an overall increase in the anode to reactor volume ratio. Additionally, this biofilm-anode suspension was capable of producing hydrogen gas when an applied potential was established across the anode and cathode, with yields approaching  $0.83 \text{ mol H}_2/\text{mol-acetate}$ <sup>26</sup>. Wu et al. compared low surface area graphite with high surface area activated carbon as a capacitive anode in a MFC. The high surface area material demonstrated higher currents (greater electricity generation). It was hypothesized that the substrate adsorbed in the micropores demonstrated lower diffusion resistances<sup>140</sup>. Deeke et al. utilized a suspension electrode to scale up an electricity producing MET system with a 2 liter anolyte, and created separate charge and discharge chambers for more efficient separation of the organic solution from the treated water<sup>28</sup>. This work highlighted the key challenges which need to be addressed in biofilm based suspension electrodes, such as bacterial adhesion, potential for electrical insulation through the biofilm, and current collector|suspension contact resistance. Overall, the use of suspension-electrodes with biofilms represents a new emerging means for scaling METs for simultaneous wastewater treatment and energy production purposes.

### 5. Theoretical and experimental approaches toward studying suspension electrode properties

From an operations point of view, suspension-based electrodes differ from insulating RFBs. RFBs operate at high flow rates to minimize current density non-uniformities<sup>141</sup> and obtain charged electrolytes by recirculating the redox- electrolyte through the charging cell multiple times<sup>10</sup>. In contrast, semi-solid flow batteries are significantly more viscous ( $\approx 1000 \text{ cP}$ ) than RFBs ( $\approx 1 \text{ cP}$ ) and suffer from significant pumping-energy dissipation at high flow rates<sup>19</sup>. It has been demonstrated that semi-solid systems operating in intermittent modes, where plugs (termed aliquots) are charged to 100% SOC in a single pass<sup>19, 24, 69, 142</sup>, are electrochemically more efficient. Undoubtedly, overcoming polarization challenges and promoting efficient utilization of the active material in a suspension electrode will require a synergistic balance between flow-properties, and suspension-electrode design. With the abundance of parameters to be considered including: electrode thickness, compositional loading, flow rate, electronic conductivity, etc., it is ideal to approach these research questions through theoretical modeling. This section highlights the coupled theoretical and experimental works related to understanding how to efficiently operate suspension-based systems.

#### 5.1 Semi-solid flow battery system modelling

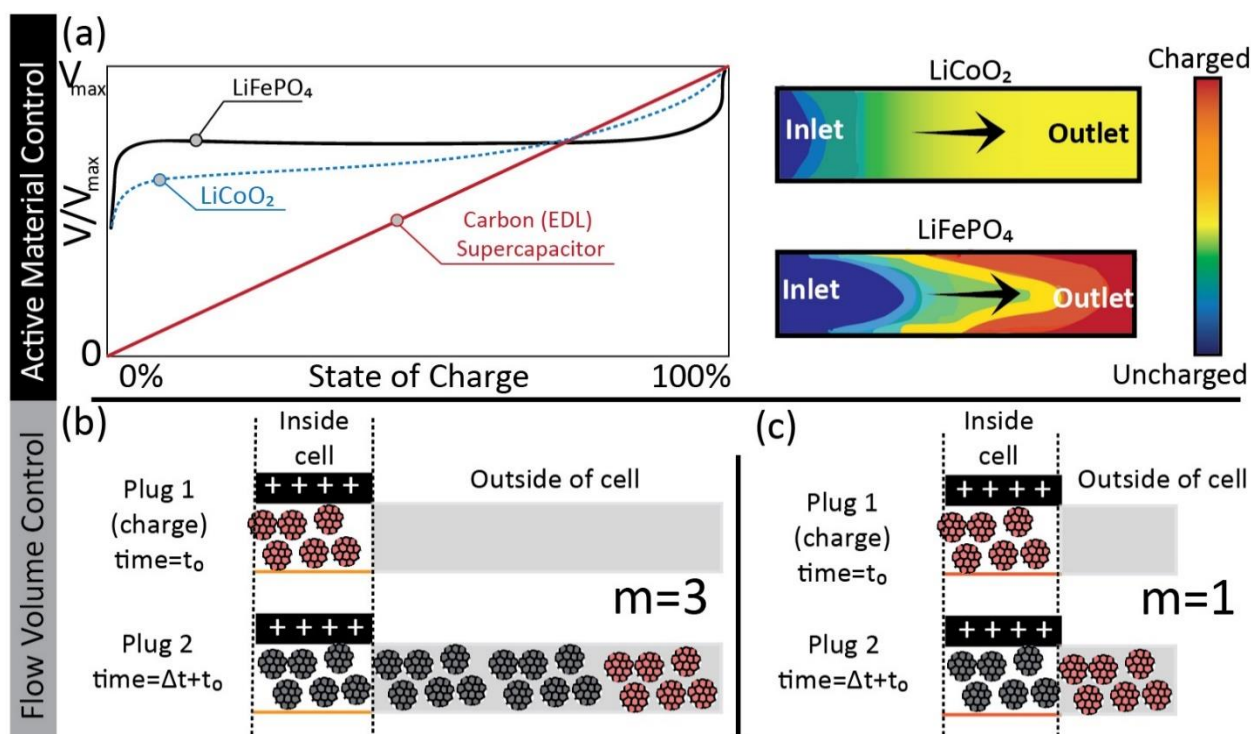


**Fig 13.** Active material control and flow volume control methods for efficient operation of suspension electrodes. Characteristic charge curve for a LiCoO<sub>2</sub>, LiFePO<sub>4</sub> and carbon based suspension electrode normalized by the maximum voltage. State of charge gradients form along the flow path with a suspension composed of LiCoO<sub>2</sub> and LiFePO<sub>4</sub> as the active material in a suspension electrode (a). Apart from controlling material properties, the way the suspension is pumped (flow volume control) can affect system performance. Two examples of pumping methods include replacing a single charged volume by 3X ( $m=3$ ) its volume (b) or 1X ( $m=1$ ) its volume (d). Figure adapted from Ref. 142 with permission from Elsevier.

Brunini et al. developed the first multi-physics based model of a SSFB<sup>142</sup>. In this model, the Doyle, Fuller, Newman (DFN)<sup>143-145</sup> porous electrode model was coupled with a non-Newtonian fluid mechanics model (Navier Stokes and Ostwald de-Waele power-law approximation<sup>146, 147</sup>) to describe the transient behavior of a SSFB composed of lithium cobalt oxide (LCO) and lithium iron phosphate (LFP) based cathodes (half-cell geometries). To account for coupled electrochemical and flow dynamics, a convection term was added to the mass transport equation in both the electrolyte and active material domains. The mathematical model was used to compare the effect of equilibrium potential (and shape of galvanostatic curve) to observed state of charge gradients during low-flow rate operating regimes. It was determined that materials that observed flatter galvanostatic curves, achieved greater current densities, and more broadly distributed state of charge (SOC) gradients across the length of the channel which led to more efficient material utilization and lower polarization. Specifically, LFP which is characterized by a flat V-t curve demonstrated a voltage efficiency (97.7%) and reached 100% SOC at the end of the simulated flow channel, whereas LCO (more curved V-t plot) only reached 70% of its theoretical capacity and has a voltage efficiency of 93.7% (Fig. 13 a). Thus, it was concluded that efficient operation requires minimizing non-uniformity of current densities across the flow channel, which can be accomplished with flat potential materials.

Material underutilization can occur because of flow mode inefficiencies. Two types of inefficiencies are: (1) electrochemical inefficiencies due to charge leakage outside the electroactive region<sup>69</sup>, and (2) charge redistribution as result of a non-uniform flow profile<sup>70</sup>. To minimize charge redistribution effects (and side-zone charging)<sup>70</sup>, it is ideal to have a suspension composition that readily slips at the wall. Li and Smith developed a computational model for

intermittent flow operation to examine the deleterious effects that occur as result of non-uniform flow operation<sup>24</sup>. A parameter called aliquot factor, designated by  $m$  was designed to assess volume control. In general,  $m=3$ , describes a scenario where a suspension volume is charged and then replaced by 3X its volume, while  $m=1$  references the operating regime where a single aliquot is charged, and then directly replaced with another aliquot (Fig. 13b). The case where  $m=3$  resulted in SOC gradients as the charged region, once pumped out the cell equilibrates and reacts with the uncharged suspension. Charge redistribution is minimized when an aliquot factor  $m=1$  is used. Later it was shown that aliquot factors  $<1$ , where flow can be described as pseudo-continuous leads to higher charge capacity and greater coulombic efficiencies when slipping occurs at the wall<sup>69</sup>. Thus, it was determined that for efficient operation of suspension electrodes it is ideal to have wall surface that enables slip, a material that exhibits a stable (flat potential), and works in a plug-flow operational mode.<sup>69</sup>

A suspension electrode's 'microstructure' refers to the solid material arrangement within an ion-containing solution. It has been shown that a suspension electrode's microstructure alters with flow-rate<sup>73, 74, 79, 93</sup> and leads to microstructural and electronic conductivity anisotropy. Olsen et al., recently examined these percolation pathways by creating a fabric-based analytical model of the conducting particle networks. In this way, they were able to derive a model for estimating the relationships between the structure and packing of active particles on tensorial electrical conductivity. The work suggests that a lattice-reduced model approach may be advantageous for examining the dynamic (and complex) aspects of flow-electrode systems.

## 5.2 Electrochemical flow capacitor system modelling

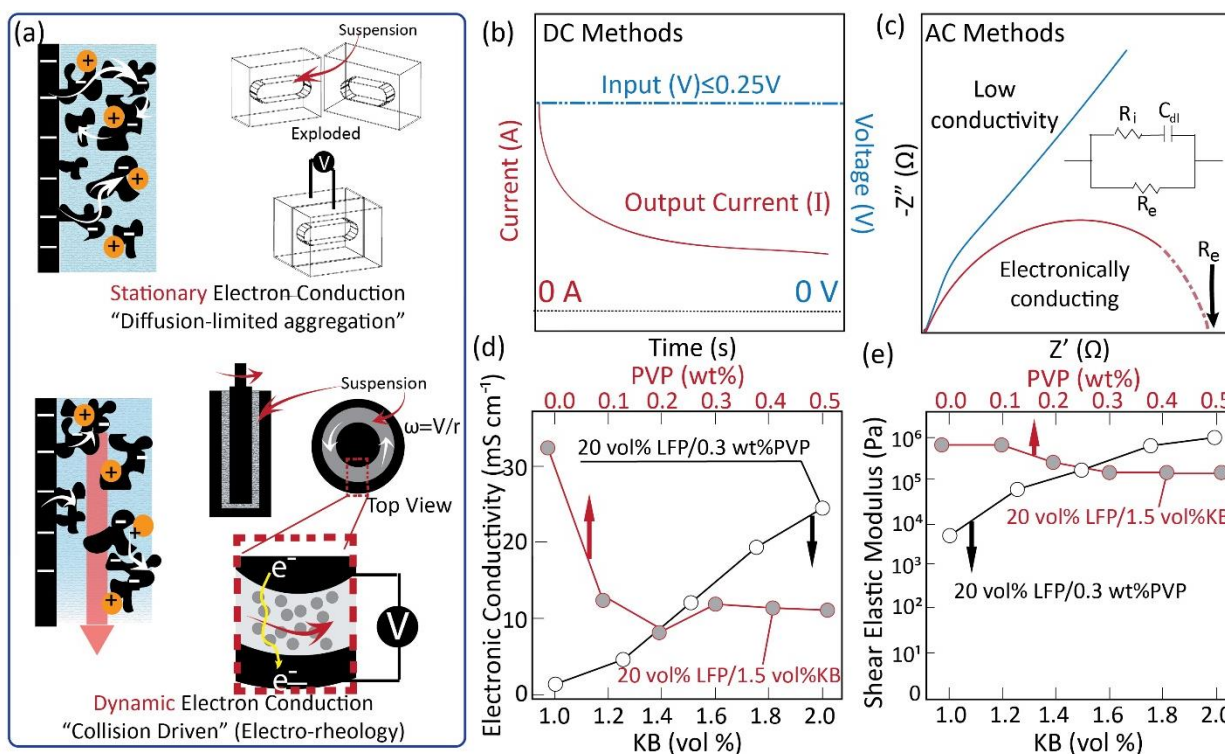


**Fig. 14.** Electron conduction via diffusion limited aggregation of the active material in a suspension electrode during static and dynamic (rheological) operations (a). The electrical conductivity can be measured using a direct current approach, where a voltage is applied across a suspension and the current response is measured (b) or with alternating current (transient) methods (c). With AC methods, the ratio between the voltage input and measured current response can be plotted on a Nyquist plot, and the electronic resistance estimated from the low frequency intercept (c). The electrical properties (d) and rheological properties (d) of a suspension electrode with varying compositions of conductive additives (Ketjen black (KB)) and non-ionic dispersant (Polyvinylpyrrolidone (PVP)). Figure adapted with permission from Ref. 156 *Advanced Energy Materials*.

Li et al. presented a generalized theoretical model of porous granular capacitive electrodes for desalination and energy storage applications<sup>148</sup>. They considered a quiescent, dilute, binary electrolyte system and utilized the Gouy-Chapman-Stern model to approximate EDL dynamics<sup>149, 150</sup>. With this model they focused on two scenarios: (1) an infinitely conducting matrix, and (2) a finite conducting matrix. In an infinitely conducting system, they demonstrate that the charging process (in terms of time) is controlled by the pore and separator resistance to ion transport. Nevertheless, in the scenario with a finite matrix conductivity there is also an associated resistance in the active material, which resists electron flow. In the latter case, they found that there is an optimal active material conductivity that minimizes the charging time of a suspension. To avoid ion depletion at the separator, it was found that it is ideal to have an active material with matching or exceeding electrical conductivity with the electrolyte.<sup>148</sup>

Hoyt et al., also used continuum modelling based on Newman's model for porous electrodes<sup>151</sup> to model the charging dynamic of an electrochemical flow capacitor<sup>152, 153</sup>. Unlike Li, Hoyt considered the dynamics scenario where the suspension was modelled as a laminar, Newtonian fluid with advection effects. In their initial study, they demonstrated similar to Li<sup>148</sup>, the importance of ionic and electronic conductivity matching. Flow results show that boundary layers were equal in magnitude when the ionic conductivity was equal to the electronic conductivity. Nevertheless, in most of the experimentally reported systems, the ionic conductivity is much greater than the electrical conductivity causing charging to only occur at the current collector, which leads to underutilization of the active material. Hoyt expanded on this work and used scaling relationships to approximate the EFCs current behavior as a function of an applied voltage. This

model was compared with experimentally obtained chronoamperometric data obtained from a single-tank electrochemical flow capacitor. The single tank EFC was constantly replenished with uncharged suspensions, and the subsequent current response was monitored for different flow rates. It was estimated that suspension electronic conductivities of 25 mS/cm (50 mS/cm in a stationary system) would be necessary to achieve a current density of 100 mA/cm<sup>2</sup> (a benchmark for realistic applications).

## 6. Rheological, physical, and electrochemical properties of suspension electrodes

In this section, we look at suspension electrodes holistically, and outline the universal material system properties that transcend specific applications. Specifically, we review the methods used for characterizing electronic, electrochemical and rheological properties of suspension electrodes.

### 6.1 Suspension electron conduction mechanisms (electrical conductivity)

Suspension electrodes have been studied in static<sup>19</sup>, intermittent<sup>69, 70, 154</sup>, and continuous<sup>78</sup> operational modes (depending on the application and experimental protocol). It has been suggested that intermittent operational modes yield the greatest energy and electrochemical efficiencies for energy storage applications<sup>24, 69, 70</sup>. In a stationary mode, the conducting material can form a three-dimensional structure which enables pathways for efficient charge transfer (Fig. 14a). The electrical conductivity of a

suspension-based electrode describes the connectivity of the active material and percolation pathways established<sup>155</sup>.

In a dynamic operation (flowing mode), the 3-D network of active particles can come apart and form large interstitial voids, which can increase the resistance (Fig. 14a). Moreover, the active material can come out of contact with the current collector, and limit electron percolation and full material utilization. Much of the physics behind particle collisions are unknown in terms of their role on ion and charge exchange and are open areas for further investigation. Electro-rheology has been the standard method for examining suspension electrode properties in a shear (or dynamic) environment. Parallel plate<sup>22</sup> and concentric cylinder<sup>67</sup> (Fig. 14a) geometries have been utilized for measuring rheological properties of suspension electrodes. AC and DC measurements can be coupled to these systems by applying an electrical potential across the sample as the inner cone or top plate rotates at varying velocities (shear rates). From these experiments, electrical conductivities can be observed as function of shear rate and voltage.

A suspension electrode's electronic conductivity can be measured under static conditions by flowing a finite-volume between two current collectors as demonstrated by the standard block arrangement in Fig. 14a<sup>18, 19</sup>. Electronic conductivities have been measured using direct current (DC) (Fig. 14 b)<sup>18, 156</sup> and alternating current (AC) methods (Fig. 14 c)<sup>19, 73, 74, 79, 93, 157</sup>. DC methods utilize a constant applied voltage and the subsequent current response is used to measure electronic conductivity. Once steady state conditions are achieved the electronic resistance can be obtained from Ohms Law<sup>78</sup>.

$$R_e = \frac{\Delta V}{\Delta I},$$

AC techniques apply an oscillating (sinusoidal) voltage across a sample and the current response is measured. The ratio between the voltage and current is the impedance (resistance) and can be plotted on a Nyquist plot (Fig. 14c). The high frequency intercept on the real axis has been reported to be a parallel combination of both the ionic and electronic resistances, and the low frequency intercept the electronic resistance<sup>19, 152</sup>. Multiple equivalent circuit models have been utilized to extract parameters such as the electronic and ionic resistances (inset Fig. 14c)<sup>73, 74, 79, 93, 157</sup>. Petek et al., examined different equivalent circuit models in order to characterize the AC response of ionic and redox-active suspensions. It was shown that the low frequency intercept (often estimated as the electronic resistances) was actually the summation of the ionic, charge transfer, and a distributed resistance, which requires a divergence from the typical Randles Circuit analyses. The distributed resistance is specific to suspension electrodes, and was minimized when ionic and electronic resistances (conductivities) were similar<sup>157</sup>. Qualitatively, a linear Nyquist plot is a signal of an insulating, or low conductivity system<sup>81</sup>, whereas a loop is indicative of greater electron percolation. The amplitude, frequency region, suspension thickness, and current collector all affect the measured resistance, and thus experimental calibration is often necessary.

The material arrangement, especially under flowing operation, dictates the electrical and electrochemical properties of a suspension electrode. Recently, Wei et al., examined and reported the electrochemical, electrical and rheological behaviours of a biphasic suspension electrodes composed of LFP and KB with and without a non-ionic dispersant (polyvinylpyrrolidone - PVP). The purpose of the additive was to tailor the material interactions within a suspension electrode. Specifically, they desired repulsive interactions between the active material (LFP), attractive interactions between the conductive additive (KB), and repulsive behaviour between the LFP

and KB materials. In general, increasing the KB concentration led to an increase in the electronic conductivity and shear elastic modulus. Increasing the PVP concentration led to a decrease in electrical conductivities and shear elastic modulus in a suspension electrode (Fig. 14d and e).<sup>156</sup>

## 6.2 Electrochemical characterization of suspension electrodes

The most common experimental tests for suspension electrodes are static electrochemistry experiments. Static or stationary tests are usually done in a symmetric two-electrode configuration (Fig. 14a). Channels for the suspension are formed either directly into the current collector (as a groove) or through the use of gaskets. Gravimetrically equal amounts of suspensions are placed in the anode and cathode compartment and then the cell is assembled with a separator between the anode and cathode compartment. It is important to note the effect of contact resistance, and the cell needs to be assembled in a way that ensures adequate contact. In non-aqueous suspension electrodes, such as those seen in the semi-solid battery, modified Swagelok cells have also been utilized. In these set-ups there is a compartment in the current collector for the cathodic suspension, and the other half of the cell is set aside for a lithium metal or another counter electrode.

Intermittent flow experiments allow for electrochemical characterization under realistic flow conditions<sup>24, 70, 75</sup>. The semi-solid flow battery and electrochemical flow capacitor both utilize intermittent flow-tests coupled with chronoamperometric electrochemical tests in order to estimate suspension capacity (Fig. 15a). In this test, uncharged suspensions are simultaneously pumped into the electroactive region via controlled syringes (Fig. 15b). The samples are then charged at a set voltage and then pumped out of the cell. After a set period of time, the suspension is reversed back into the cell and discharged at 0 V. The resulting chronoamperometric profile can be examined to calculate the electrochemical performance of the flowable electrode under intermittent flow-mode (Fig. 15a). In general, the discharge curve is used in for calculating the gravimetric capacitance (EFC)/capacity (SSFB).

## 6.3 Mechanical and structural properties of suspension electrodes

For complex fluids and material systems, oscillatory or non-steady state (dynamic) rheological techniques are used to probe mechanical properties. Oscillatory techniques enable characterization of structural and dynamic properties of suspension electrodes at different time scales, which can lead to a deeper understanding of how the microstructure (arrangement of active material) and associated changes with flow rate. Traditionally, oscillatory techniques use similar geometries as seen the steady shear experiments (Fig. 14c). However, in oscillatory shear experiments, instead of stepping shear rates, and measuring viscosity the suspension electrode is placed between concentric cylinders (or parallel plates) and exposed to oscillatory strain perturbations. The relationship between the oscillatory strain and stress measurements (in terms of phase) can lead to qualitative descriptions of the particle arrangement in a suspension electrode.

## 7. Discussion and Outlook

Grid energy storage has fundamentally been hindered by limitations in traditional sodium-sulfur lead-acid, and redox flow batteries. Moreover, scaling up energy dense Li-ion batteries and power-dense supercapacitors is challenging because the inactive material cost directly scale with system capacity. The use of suspension electrodes allows for bypassing these traditional limitations by using a wider spectrum of materials suspended in an electrolyte to form a flowable multiphase material system<sup>38</sup>. This

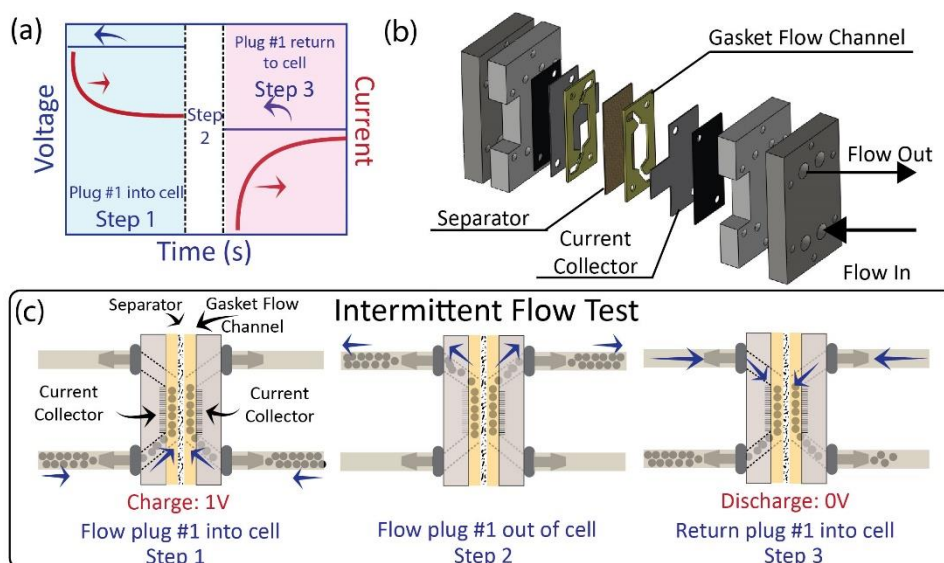


**Fig. 15.** An example of chronoamperometric data obtained from an intermittent flow experiment (a) used to study the ability for a suspension electrode to flow and store charge. In operation, a flow cell is utilized for charging suspensions in continuous and intermittent operational modes (b). Intermittent flow experiments are conducted according to (c). In practice, suspensions are pumped into the cell and charged until the current decays to close to 0 A. Then the volume is removed from the cell, and then returned to the cell and discharged at 0V.

premise opens up a range of material chemistries that can be examined in a host of applications. Such material chemistries include, intercalation chemistries (metal-oxides)<sup>19</sup>, dissolution-precipitation systems<sup>101, 102</sup>, electrodeposition (metal-based RFBs), and electrochemical capacitors<sup>21</sup>. Hybrid<sup>6, 20, 121</sup> and asymmetric<sup>71</sup> systems which utilize various types of charge storage mechanisms can also be used. Moreover, capacitive suspension electrodes have been demonstrated in a range of applications related to water – water treatment<sup>26, 27</sup>, capacitive deionization<sup>13, 14, 16</sup>, and energy generation from salinity gradients<sup>129</sup>.

The versatility of these systems offers tremendous promise, but the methods and best practices are far from perfect. As a material system, we are concerned with not only the active material's properties, but also how the active material can be synergistically combined with an ionic solution and a conductive additive. While it has been demonstrated that charge percolation occurs at very small contents of conductive additives<sup>22, 79</sup>, it has also been reported that conductivity can be significantly decreased during flowing operation<sup>74, 79, 93</sup>. High additive loading diminishes energy storage capacities, and increases the viscosity of a suspension electrode<sup>23</sup>. Thus, while the addition of conductive additive is often inferred as obvious in conventional systems, its role in suspension electrodes is far from intuitive. Thus, novel methods that minimize the use of a conductive additive yet promote electron transport are of interest. Specifically the exploration into novel redox shuttle molecules<sup>94</sup>, redox-active colloid systems, and polymer brush-based systems are of interest.

Throughout this review, we emphasize the importance of tailoring materials and suspension electrodes to a desired application. Design requires a coalescence of rheology, electrochemistry, and aspects of colloidal science, in order to best devise an active material that enables either efficient ion removal, biofilm growth, or energy storage properties. The suspension electrode performance is not only controlled by the active material, but also by the active material arrangement (and connectivity) throughout a suspension electrode. Active material size and

morphology (spherical vs. anisometric) play a critical role in the flowability, diffusion limited aggregation effects, and overall material utilization. Material utilization is and will be a continued research area, as large over-potentials and system resistances limit the electrochemical efficiency and contribute to mechanical and electrical inefficiencies. It is expected that tailored flow designs and a divergence from a typical flow architecture may yield methods for overall material and systems level improvements in terms of efficiency<sup>69, 70</sup>.

For large-scale grid energy storage, suspension electrodes based on low-cost and abundant materials are necessary. Moreover, systems need to be able to hold charge for extended periods of time (at least 2-12 hours). Thus, all suspension electrodes based on different chemistries need to be better understood in terms of self-discharge properties. For applications such as those seen in water technologies, low cost and low energy consumption are required in order to compete with existing technologies. Specifically, improvements in energy recovery from capacitive suspension electrodes used in ion removal processes is needed. Improvements in energy recovery will come with more expansive knowledge on engineering parameters such as the effects of feedwater flow-rate, solid and electrolyte concentrations, and trade-offs between electrical and pumping energy requirements. Nevertheless, as new methods and best practices are established, it is expected that this field will see significant growth. Full acceleration will require joint efforts from experts from a range of disciplines including material science, fluid mechanics, electrochemistry, colloidal science, and engineering backgrounds. Open and relevant research questions and areas that need to be addressed include:

(1) Novel *in-situ* and *in-operando* characterization techniques to probe fundamental aspects of suspension electrode behavior on the micro- and nanoscale level. Specifically understanding ion and electron percolation pathways and exchange mechanisms are of interest.

(2) Understanding particle re-arrangement properties during shear modes are of interest for designing electrically conducting

networks for both capacitive deionization and grid energy storage applications. Moreover there is a need to understand how particle arrangement affects the electrochemical properties of a suspension electrode.

(3) Understanding how charge and ion redistribution occur in suspension electrodes during storage, and how charging rate contributes to these dynamics.

(4) Understanding how the over-potentials can be decreased for efficient and optimal material utilization in thick suspension electrodes.

(5) Investigations into the design of novel redox-shuttle molecules that enable charging of the active material in a suspension electrode while limiting the need or conductive additives and decreasing the overall suspension electrode viscosity.

(6) In depth studies on the rheological properties of suspension electrodes that eliminate shear-banding in concentrated systems while mitigate pumping requirements. Moreover, active material arrangement via an external stimuli (pH, voltage, temperature inputs) is of interest for more advanced and tunable systems.

(7) Multi-scale modelling of charge-discharge dynamic and transient physical properties in a charge suspension (flow-electrode) should allow accelerated selection of materials and design of flowable electrode and systems that utilize them.

## 7. Acknowledgements

This work was supported as part of the Fluid Interface Reactions, Structures and Transport (FIRST) Center, an Energy Frontier Research Center funded by the U.S. Department of Energy, Office of Science, Basic Energy Sciences under Award no. ERKCC61. KBH was supported by the NSF Graduate Research Fellowship (Grant# 1002809).

## Bibliography

- 1.M. Elimelech and W. A. Phillip, *Science*, 2011, **333**, 712-717.
- 2.M. A. Shannon, P. W. Bohn, M. Elimelech, J. G. Georgiadis, B. J. Mariñas and A. M. Mayes, *Nature*, 2008, **452**, 301-310.
- 3.D. Hostick, D. Belzer, S. Hadley, T. Markel, C. Marnay and M. Kintner-Meyer, *Renewable Electricity Futures Study. Volume 3: End-Use Electricity Demand (Report)*, National Renewable Energy Laboratory (NREL), Golden, CO., 2012.
- 4.B. E. Logan and K. Rabaey, *Science*, 2012, **337**, 686-690.
- 5.B. Dunn, H. Kamath and J.-M. Tarascon, *Science*, 2011, **334**, 928-935.
- 6.K. B. Hatzell, M. Boota, E. C. Kumbur and Y. Gogotsi, *Journal of The Electrochemical Society*, 2015, **162**, A5007-A5012.
- 7.Z. Yang, J. Zhang, M. C. Kintner-Meyer, X. Lu, D. Choi, J. P. Lemmon and J. Liu, *Chemical Reviews*, 2011, **111**, 3577-3613.
- 8.C. J. Barnhart and S. M. Benson, *Energy & Environmental Science*, 2013, **6**, 1083-1092.
- 9.J. Whitacre, T. Wiley, S. Shanbhag, Y. Wenzhuo, A. Mohamed, S. Chun, E. Weber, D. Blackwood, E. Lynch-Bell and J. Gulakowski, *Journal of Power Sources*, 2012, **213**, 255-264.
- 10.A. Z. Weber, M. M. Mench, J. P. Meyers, P. N. Ross, J. T. Gostick and Q. Liu, *Journal of Applied Electrochemistry*, 2011, **41**, 1137-1164.
- 11.M. Skyllas-Kazacos, M. Chakrabarti, S. Hajimolana, F. Mjalli and M. Saleem, *Journal of the Electrochemical Society*, 2011, **158**, R55-R79.
- 12.M. Skyllas-Kazacos, M. Rychcik, R. G. Robins, A. Fane and M. Green, *Journal of the Electrochemical Society*, 1986, **133**, 1057-1058.
- 13.S.-I. Jeon, H.-R. Park, J.-G. Yeo, S. Yang, C. H. Cho, M. H. Han and D.-K. Kim, *Energy & Environmental Science*, 2013, **6**, 1471-1475.
- 14.S.-I. Jeon, J.-G. Yeo, S. Yang, J. Choi and D. K. Kim, *Journal of Materials Chemistry A*, 2014, **2**, 6378-6383.
- 15.K. B. Hatzell, M. C. Hatzell, K. M. Cook, M. Boota, G. M. Housel, A. McBride, E. C. Kumbur and Y. Gogotsi, *Environmental Science & Technology*, 2015, **49**, 3040-3047.
- 16.K. B. Hatzell, E. Iwama, A. Ferris, B. Daffos, K. Urita, T. Tzedakis, F. Chauvet, P.-L. Taberna, Y. Gogotsi and P. Simon, *Electrochemistry Communications*, 2014, **43**, 18-21.
- 17.Y. Gendel, A. K. E. Rommerskirchen, O. David and M. Wessling, *Electrochemistry Communications*, 2014, **46**, 152-156.
- 18.S. Porada, D. Weingarth, H. V. Hamelers, M. Bryjak, V. Presser and P. Biesheuvel, *Journal of Materials Chemistry A*, 2014, **2**, 9313-9321.
- 19.M. Duduta, B. Ho, V. C. Wood, P. Limthongkul, V. E. Brunini, W. C. Carter and Y. M. Chiang, *Advanced Energy Materials*, 2011, **1**, 511-516.
- 20.K. B. Hatzell, M. Beidaghi, J. W. Campos, C. R. Dennison, E. C. Kumbur and Y. Gogotsi, *Electrochimica Acta*, 2013, **111**, 888-897.
- 21.V. Presser, C. R. Dennison, J. Campos, K. W. Knehr, E. C. Kumbur and Y. Gogotsi, *Advanced Energy Materials*, 2012, **2**, 895-902.
- 22.F. Y. Fan, W. H. Woodford, Z. Li, N. Baram, K. C. Smith, A. Helal, G. H. McKinley, W. C. Carter and Y.-M. Chiang, *Nano Letters*, 2014, **14**, 2210-2218.
- 23.S. Hamelet, T. Tzedakis, J.-B. Leriche, S. Sailer, D. Larcher, P.-L. Taberna, P. Simon and J.-M. Tarascon, *Journal of The Electrochemical Society*, 2012, **159**, A1360-A1367.
- 24.Z. Li, K. C. Smith, Y. Dong, N. Baram, F. Y. Fan, J. Xie, P. Limthongkul, W. C. Carter and Y.-M. Chiang, *Physical Chemistry Chemical Physics*, 2013, **15**, 15833-15839.
- 25.M. Hatzell, K. B. Hatzell and B. E. Logan, *Environmental Science & Technology Letters*, 2014, **12**, 474-478.
- 26.J. Liu, F. Zhang, W. He, W. Yang, Y. Feng and B. E. Logan, *Journal of Power Sources*, 2014, **271**, 530-533.
- 27.J. Liu, F. Zhang, W. He, X. Zhang, Y. Feng and B. E. Logan, *Journal of Power Sources*, 2014, **261**, 278-284.
- 28.A. Deeke, T. H. Sleutels, T. F. Donkers, H. V. Hamelers, C. J. Buisman and A. Ter Heijne, *Environmental Science & Technology*, 2015.
- 29.N. Shvab, N. Stefanjak, K. Kazdobin and A. Wragg, *Journal of Applied Electrochemistry*, 2000, **30**, 1285-1292.
- 30.N. Shvab, N. Stefanjak, K. Kazdobin and A. Wragg, *Journal of Applied Electrochemistry*, 2000, **30**, 1293-1298.
- 31.J. Iza, *Water Science & Technology*, 1991, **24**, 109-132.
- 32.A. A. Van de Graaf, P. de Bruijn, L. A. Robertson, M. S. Jetten and J. G. Kuenen, *Microbiology*, 1996, **142**, 2187-2196.
- 33.R. Oriňáková, H.-D. Wiemhöfer, J. Paulsdorf, V. Barinková, A. Bednáríková and R. M. Smith, *Journal of Solid State Electrochemistry*, 2006, **10**, 458-464.
- 34.W. Sherwood, P. Queneau, C. Nikolic and D. Hodges, *Metallurgical Transactions B*, 1979, **10**, 659-666.
- 35.B. Sabacky and J. Evans, *Metallurgical Transactions B*, 1977, **8**, 5-13.
- 36.D. S. Flett, *Industrial and Engineering Chemistry*, 1971, 300-312.
- 37.J. Backhurst, J. Coulson, F. Goodridge, R. Plimley and M. Fleischmann, *Journal of the Electrochemical Society*, 1969, **116**, 1600-1607.
- 38.D. Kastening, W. Schiel and M. Henschel, *Journal of Electroanalytical Chemistry*, 1985, **191**, 311-328.
- 39.B. Kastening and S. Spinzig, *Journal of Electroanalytical Chemistry and Interfacial Electrochemistry*, 1986, **214**, 295-302.
- 40.S. Gu, K. Gong, E. Z. Yan and Y. Yan, *Energy & Environmental Science*, 2014, **7**, 2986-2998.

- 41.L. Li, S. Kim, W. Wang, M. Vijayakumar, Z. Nie, B. Chen, J. Zhang, G. Xia, J. Hu and G. Graff, *Advanced Energy Materials*, 2011, **1**, 394-400.
- 42.R. M. Darling, K. G. Gallagher, J. A. Kowalski, S. Ha and F. R. Brushett, *Energy & Environmental Science*, 2014, **7**, 3459-3477.
- 43.G. Kear, A. A. Shah and F. C. Walsh, *International Journal of Energy Research*, 2012, **36**, 1105-1120.
- 44.P. Leung, X. Li, C. P. de León, L. Berlouis, C. J. Low and F. C. Walsh, *RSC Advances*, 2012, **2**, 10125-10156.
- 45.S.-Y. Chung, J. T. Bloking and Y.-M. Chiang, *Nature Materials*, 2002, **1**, 123-128.
- 46.A. K. Padhi, K. Nanjundaswamy and J. Goodenough, *Journal of the Electrochemical Society*, 1997, **144**, 1188-1194.
- 47.S. Yang, Y. Song, P. Y. Zavalij and M. S. Whittingham, *Electrochemistry Communications*, 2002, **4**, 239-244.
- 48.Y. M. Chiang, W. H. Woodford, F. Y. Fan, Z. Li, N. Baram, K. C. Smith, W. C. Carter, G. H. Mckinley and A. Helal, 2014.
- 49.B. Li, Z. Nie, M. Vijayakumar, G. Li, J. Liu, V. Sprenkle and W. Wang, *Nature communications*, 2015, **6**.
- 50.K. L. Hawthorne, T. J. Petek, M. A. Miller, J. S. Wainright and R. F. Savinell, *Journal of The Electrochemical Society*, 2015, **162**, A108-A113.
- 51.P. Simon and Y. Gogotsi, *Nature Materials*, 2008, **7**, 845-854.
- 52.P. Simon and Y. Gogotsi, *Accounts of Chemical Research*, 2012, **46**, 1094-1103.
- 53.Y. Zhao, S. Si and C. Liao, *Journal of Power Sources*, 2013, **241**, 449-453.
- 54.S. Wu, Y. Zhao, D. Li, Y. Xia and S. Si, *Journal of Power Sources*, 2015, **275**, 305-311.
- 55.Y. Zhao, S. Si, L. Wang, C. Liao, P. Tang and H. Cao, *Journal of Power Sources*, 2014, **248**, 962-968.
- 56.A. J. Bard and L. R. Faulkner, *Electrochemical methods: fundamentals and applications*, Wiley New York, 1980.
- 57.B. E. Conway, *Journal of the Electrochemical Society*, 1991, **138**, 1539-1548.
- 58.P. Simon, Y. Gogotsi and B. Dunn, *Science Magazine*, 2014, **343**, pp. 1210-1211.
- 59.E. Frackowiak and F. Beguin, *Carbon*, 2001, **39**, 937-950.
- 60.D. Brogioli, R. Ziano, R. Rica, D. Salerno, O. Kozynchenko, H. Hamelers and F. Mantegazza, *Energy & Environmental Science*, 2012, **5**, 9870-9880.
- 61.R. Rica, R. Ziano, D. Salerno, F. Mantegazza and D. Brogioli, *Physical review letters*, 2012, **109**, 156103.
- 62.S. Porada, L. Borhardt, M. Oschatz, M. Bryjak, J. Atchison, K. Keesman, S. Kaskel, P. Biesheuvel and V. Presser, *Energy & Environmental Science*, 2013, **6**, 3700-3712.
- 63.M. C. Hatzell, M. Raju, V. J. Watson, A. G. Stack, A. C. van Duin and B. E. Logan, *Environmental Science & Technology*, 2014, **48**, 14041-14048.
- 64.H. Liu and B. E. Logan, *Environmental Science & Technology*, 2004, **38**, 4040-4046.
- 65.H. Liu, R. Ramnarayanan and B. E. Logan, *Environmental Science & Technology*, 2004, **38**, 2281-2285.
- 66.P. Yang and J.-M. Tarascon, *Nature Materials*, 2012, **11**, 560-563.
- 67.J. W. Campos, M. Beidaghi, K. B. Hatzell, C. R. Dennison, B. Musci, V. Presser, E. C. Kumbur and Y. Gogotsi, *Electrochimica Acta*, 2013, **98**, 123-130.
- 68.A. Zocchi, 2004.
- 69.K. C. Smith, Y.-M. Chiang and W. C. Carter, *Journal of The Electrochemical Society*, 2014, **161**, A486-A496.
- 70.K. C. Smith, V. E. Brunini, Y. Dong, Y.-M. Chiang and W. C. Carter, *Electrochimica Acta*, 2014, **147**, 460-469.
- 71.K. B. Hatzell, L. Fan, M. Beidaghi, M. Boota, E. Pomerantseva, E. C. Kumbur and Y. Gogotsi, *ACS applied materials & interfaces*, 2014, **6**, 8886-8893.
- 72.B. Kastening, N. Busscher and U. Asskamp, *Journal of Electroanalytical Chemistry and Interfacial Electrochemistry*, 1989, **265**, 77-101.
- 73.L. Madec, M. Youssry, M. Cerbelaud, P. Soudan, D. Guyomard and B. Lestriez, *Journal of The Electrochemical Society*, 2014, **161**, A693-A699.
- 74.L. Madec, M. Youssry, M. Cerbelaud, P. Soudan, D. Guyomard and B. Lestriez, *ChemPlusChem*, 2014, **80**, 396-401.
- 75.M. Boota, K. Hatzell, M. Beidaghi, C. Dennison, E. Kumbur and Y. Gogotsi, *J. Electrochem. Soc.*, 2014, **161**, A1078-A1083.
- 76.S. Sasi, A. Murali, S. V. Nair, A. S. Nair and K. Subramanian, *Journal of Materials Chemistry A*, 2015, 2717-2725.
- 77.M. Boota, K. B. Hatzell, M. Alhabeb, E. C. Kumbur and Y. Gogotsi, *Carbon*, 2015, **92**, 142-149.
- 78.S. Porada, J. Lee, D. Weingarth and V. Presser, *Electrochemistry Communications*, 2014, **48**, 178-181.
- 79.M. Youssry, L. Madec, P. Soudan, M. Cerbelaud, D. Guyomard and B. Lestriez, *Physical Chemistry Chemical Physics*, 2013, **15**, 14476-14486.
- 80.M. D. Stoller and R. S. Ruoff, *Energy & Environmental Science*, 2010, **3**, 1294-1301.
- 81.M. Cerbelaud, B. Lestriez, R. Ferrando, A. Videcoq, M. Richard-Plouet, M. Teresa Caldes and D. Guyomard, *Langmuir*, 2014, **30**, 2660-2669.
- 82.R. I. Tanner, *Engineering rheology*, Oxford University Press, New York, 2000.
- 83.H. A. Barnes, J. F. Hutton and K. Walters, *An introduction to rheology*, Elsevier, Amsterdam, The Netherlands, 1989.
- 84.F. Boylu, H. Dincer and G. Ateşok, *Fuel Processing Technology*, 2004, **85**, 241-250.
- 85.C. Zhang, K. B. Hatzell, M. Boota, B. Dyatkin, M. Beidaghi, D. Long, W. Qiao, E. C. Kumbur and Y. Gogotsi, *Carbon*, 2014, **77**, 155-164.
- 86.E. Peled, *Journal of The Electrochemical Society*, 1979, **126**, 2047-2051.
- 87.K. B. Hatzell, A. Sharma and H. K. Fathy, 2012.
- 88.E. Ventosa, G. Zampardi, C. Flox, F. La Mantia, W. Schuhmann and J. Morante, *Chemical Communications*, 2015.
- 89.K. Colbow, J. Dahn and R. Haering, *Journal of Power Sources*, 1989, **26**, 397-402.
- 90.T. Brousse, P. Fragnaud, R. Marchand, D. Schleich, O. Bohnke and K. West, *Journal of power sources*, 1997, **68**, 412-415.
- 91.E. Ventosa, M. Skoumal, F. J. Vazquez, C. Flox, J. Arbiol and J. R. Morante, *ChemSusChem*, 2015, **8**, 1737-1744. .
- 92.D. Young, A. Ransil, R. Amin, Z. Li and Y. M. Chiang, *Advanced Energy Materials*, 2013, **3**, 1125-1129.
- 93.M. Youssry, L. Madec, P. Soudan, M. Cerbelaud, D. Guyomard and B. Lestriez, *Journal of Power Sources*, 2015, **274**, 424-431.
- 94.Q. Huang, H. Li, M. Grätzel and Q. Wang, *Physical Chemistry Chemical Physics*, 2013, **15**, 1793-1797.
- 95.H. Zhang, X. Yu and P. V. Braun, *Nature Nanotechnology*, 2011, **6**, 277-281.
- 96.M. Ebner, D. W. Chung, R. E. García and V. Wood, *Advanced Energy Materials*, 2014, **4**.
- 97.B. L. Ellis and L. F. Nazar, *Current Opinion in Solid State and Materials Science*, 2012, **16**, 168-177.
- 98.J. Whitacre, A. Tevar and S. Sharma, *Electrochemistry Communications*, 2010, **12**, 463-466.

- 99.E. Ventosa, D. Buchholz, S. Klink, C. Flox, L. G. Chagas, C. Vaalma, W. Schuhmann, S. Passerini and J. R. Morante, *Chemical Communications*, 2015.
- 100.D. Buchholz, A. Moretti, R. Kloepsch, S. Nowak, V. Siozios, M. Winter and S. Passerini, *Chemistry of Materials*, 2013, **25**, 142-148.
- 101.A. Manthiram, Y. Fu and Y.-S. Su, *Accounts of Chemical Research*, 2012, **46**, 1125-1134.
- 102.Y. Yang, G. Zheng and Y. Cui, *Energy & Environmental Science*, 2013, **6**, 1552-1558.
- 103.G. Zhou, S. Pei, L. Li, D. W. Wang, S. Wang, K. Huang, L. C. Yin, F. Li and H. M. Cheng, *Advanced Materials*, 2014, **26**, 625-631.
- 104.X. Ji and L. F. Nazar, *Journal of Materials Chemistry*, 2010, **20**, 9821-9826.
- 105.F. Y. Fan, W. C. Carter and Y. M. Chiang, *Advanced Materials*, 2015.
- 106.H. Pan, X. Wei, W. A. Henderson, Y. Shao, J. Chen, P. Bhattacharya, J. Xiao and J. Liu, *Advanced Energy Materials*, 2015, DOI: 10.1002/aenm.201500113.
- 107.R. Rauh, F. Shuker, J. Marston and S. Brummer, *Journal of Inorganic and Nuclear Chemistry*, 1977, **39**, 1761-1766.
- 108.F. Fan, W. Woodford, Z. Li, N. Baram, K. C. Smith, A. Helal, G. H. McKinley, W. C. Carter and Y.-M. Chiang, *Nano Lett.*, 2014, **14** 2210-2218.
- 109.H. Chen, Q. Zou, Z. Liang, H. Liu, Q. Li and Y.-C. Lu, *Nature communications*, 2015, **6**.
- 110.V. Khomenko, E. Raymundo-Pinero and F. Béguin, *Journal of Power Sources*, 2006, **153**, 183-190.
- 111.K. Fic, G. Lota, M. Meller and E. Frackowiak, *Energy & Environmental Science*, 2012, **5**, 5842-5850.
- 112.K. Hernández-Burgos, S. E. Burkhardt, G. G. Rodríguez-Calero, R. G. Hennig and H. D. Abreuña, *The Journal of Physical Chemistry C*, 2014, **118**, 6046-6051.
- 113.B. Huskinson, M. P. Marshak, C. Suh, S. Er, M. R. Gerhardt, C. J. Galvin, X. Chen, A. Aspuru-Guzik, R. G. Gordon and M. J. Aziz, *Nature*, 2014, **505**, 195-198.
- 114.B. Yang, L. Hooper-Burkhardt, F. Wang, G. S. Prakash and S. Narayanan, *Journal of The Electrochemical Society*, 2014, **161**, A1371-A1380.
- 115.G. Pognon, T. Brousse, L. Demarconnay and D. Bélanger, *Journal of Power Sources*, 2011, **196**, 4117-4122.
- 116.G. Pognon, T. Brousse and D. Bélanger, *Carbon*, 2011, **49**, 1340-1348.
- 117.M. Weissmann, O. Crosnier, T. Brousse and D. Bélanger, *Electrochimica Acta*, 2012, **82**, 250-256.
- 118.D. M. Anjos, J. K. McDonough, E. Perre, G. M. Brown, S. H. Overbury, Y. Gogotsi and V. Presser, *Nano Energy*, 2013, **2**, 702-712.
- 119.S. Roldán, C. Blanco, M. Granda, R. Menéndez and R. Santamaría, *Angewandte Chemie International Edition*, 2011, **50**, 1699-1701.
- 120.S. Roldán, M. Granda, R. Menéndez, R. Santamaría and C. Blanco, *The Journal of Physical Chemistry C*, 2011, **115**, 17606-17611.
- 121.M. Boota, K. Hatzell, E. Kumbur and Y. Gogotsi, *ChemSusChem*, 2015, **8**, 835-843.
- 122.S. Roldán, Z. González, C. Blanco, M. Granda, R. Menéndez and R. Santamaría, *Electrochimica Acta*, 2011, **56**, 3401-3405.
- 123.Z. Liu, H. Zhou, Z. Huang, W. Wang, F. Zeng and Y. Kuang, *Journal of Materials Chemistry A*, 2013, **1**, 3454-3462.
- 124.H. Yu, L. Fan, J. Wu, Y. Lin, M. Huang, J. Lin and Z. Lan, *RSC Adv.*, 2012, **2**, 6736-6740.
- 125.M. Boota, K. Hatzell, E. Kumbur and Y. Gogotsi, *ChemSusChem*, 2015.
- 126.S. Müller, F. Holzer and O. Haas, *Journal of Applied Electrochemistry*, 1998, **28**, 895-898.
- 127.T. J. Petek, N. C. Hoyt, R. F. Savinell and J. S. Wainright, *Journal of Power Sources*, 2015, **294**, 620-626.
- 128.S. Porada, R. Zhao, A. Van Der Wal, V. Presser and P. Biesheuvel, *Progress in Materials Science*, 2013, **58**, 1388-1442.
- 129.M. C. Hatzell, K. B. Hatzell and B. E. Logan, *Environmental Science & Technology Letters*, 2014, **1**, 474-478.
- 130.P. Biesheuvel, R. Zhao, S. Porada and A. Van der Wal, *Journal of Colloid and Interface Science*, 2011, **360**, 239-248.
- 131.P. Biesheuvel and A. Van der Wal, *Journal of Membrane Science*, 2010, **346**, 256-262.
- 132.J. C. Farmer, D. V. Fix, G. V. Mack, R. W. Pekala and J. F. Poco, *Journal of the Electrochemical Society*, 1996, **143**, 159-169.
- 133.A. Rommerskirchen, Y. Gendel and M. Wessling, *Electrochemistry Communications*, 2015, **60**, 34-37.
- 134.P. L. McCarty, J. Bae and J. Kim, *Environmental Science & Technology*, 2011, **45**, 7100-7106.
- 135.E. Heidrich, T. Curtis and J. Dolfig, *Environmental Science & Technology*, 2010, **45**, 827-832.
- 136.U. Schröder, F. Harnisch and L. T. Angenent, *Energy & Environmental Science*, 2015, **8**, 513-519.
- 137.B. Logan, S. Cheng, V. Watson and G. Estadt, *Environmental Science & Technology*, 2007, **41**, 3341-3346.
- 138.B. E. Logan, *Applied Microbiology and Biotechnology*, 2010, **85**, 1665-1671.
- 139.K. Kida, S. Morimura, Y. Sonoda, M. Obe and T. Kondo, *Journal of Fermentation and Bioengineering*, 1990, **69**, 354-359.
- 140.S. Wu, P. Liang, C. Zhang, H. Li, K. Zuo and X. Huang, *Electrochimica Acta*, 2015, **161**, 245-251.
- 141.C. P. De Leon, A. Frías-Ferrer, J. González-García, D. Szánto and F. C. Walsh, *Journal of Power Sources*, 2006, **160**, 716-732.
- 142.V. E. Brunini, Y.-M. Chiang and W. C. Carter, *Electrochimica Acta*, 2012, **69**, 301-307.
- 143.J. Newman and W. Tiedemann, *AIChE Journal*, 1975, **21**, 25-41.
- 144.T. F. Fuller, M. Doyle and J. Newman, *Journal of the Electrochemical Society*, 1994, **141**, 1-10.
- 145.M. Doyle, J. Newman, A. S. Gozdz, C. N. Schmutz and J. M. Tarascon, *Journal of the Electrochemical Society*, 1996, **143**, 1890-1903.
- 146.J. L. Doublier, *Starch-Stärke*, 1981, **33**, 415-420.
- 147.W. Kozicki, C. Chou and C. Tiu, *Chemical Engineering Science*, 1966, **21**, 665-679.
- 148.M. Li, H. Hu and H. H. Bau, *Physical Chemistry Chemical Physics*, 2015.
- 149.P. Biesheuvel and M. Bazant, *Physical review E*, 2010, **81**, 031502.
- 150.J. O. M. Bockris and A. K. Reddy, *Modern electrochemistry: an introduction to an interdisciplinary area*, Springer Science & Business Media, 1973.
- 151.A. Johnson and J. Newman, *Journal of the Electrochemical Society*, 1971, **118**, 510-517.
- 152.N. C. Hoyt, J. S. Wainright and R. F. Savinell, *Journal of The Electrochemical Society*, 2015, **162**, A652-A657.
- 153.N. C. Hoyt, J. S. Wainright and R. F. Savinell, *Journal of The Electrochemical Society*, 2015, **162**, A1102-A1110.
- 154.C. Dennison, M. Beidaghi, K. Hatzell, J. Campos, Y. Gogotsi and E. Kumbur, *Journal of Power Sources*, 2014, **247**, 489-496.
- 155.T. Olsen and K. Kamrin, *arXiv preprint arXiv:1501.03096*, 2015.
- 156.T. S. Wei, F. Y. Fan, A. Helal, K. C. Smith, G. H. McKinley, Y. M. Chiang and J. A. Lewis, *Advanced Energy Materials*, 2015.
- 157.T. J. Petek, N. C. Hoyt, R. F. Savinell and J. S. Wainright, 2016, **163**, A5001-A5009.

